2005

The Quantum Dynamics of H2 in a C60 Lattice

Christie Simmons
Oberlin College

The Quantum Dynamics of H_2 in a C_{60} Lattice

An Honors Thesis Presented to the

Physics Department of Oberlin College

by

Christie Simmons

April 18, 2005

Contents

List of Figures

Acknowledgements

I would like to thank the following people:

My advisor, Professor Stephen FitzGerald, for his support and guidance, and for his willingness, ability, and patience to answer all of my many questions.

Fellow students, Hugh Churchill and Phil Korngut, whose work in the lab was invaluable for producing the results in this paper, and who continued to provide a source of intellectual dialogue, companionship, and entertainment.

Bill Martin for his many hours of work to create "the box" and for his help to make a seemingly never-ending series of adjustments to it.

The Oberlin College Department of Physics and Astronomy.

Chapter 1

Introduction

Since its onset in 1941, matrix isolation has become a popular and common technique for studying species using spectroscopy by isolating them in an inert host solid [1]. Due to the large, spherical shape of the molecules, solid C_{60} has large interstitial voids making it a good host for matrix isolation. These voids come in two varieties. The larger of the two, the octahedral sites, have an ideal size for studying the dynamics of H_2 molecules because the sites are large enough that a hydrogen molecule can be trapped, resulting in quantized translational motion, and can rotate nearly freely within the site. On the other hand, the sites are also small enough that each will contain only one hydrogen molecule thus eliminating H_2-H_2 interactions. The dynamics of a single hydrogen molecule isolated within the potential well of an octahedral site are very interesting because it represents a real-life example of the famous quantum mechanical situation of a "particle-in-a-box".

While the quantum dynamics of hydrogen within a C_{60} host lattice is worthy of investigation purely on the basis of the interesting physics involved in the system, there is also a practical importance for gaining a better understanding of the C_{60}-H_2, host-guest interaction because of the continuing interest in the possible use of carbon nanostructures as devices for hydrogen storage [2, 3]. Using infrared spectroscopy to study H_2 intercalated within a C_{60} lattice gives insight into the nature of the C_{60}-H_2 interaction because H_2 is not infrared-active under normal conditions and so the H_2 absorption peaks in our spectra are purely due to interaction with the C_{60} host. Initial results of the H_2 absorbance spectrum were published in 2002 by Professor Stephen FitzGerald, Scott Forth, and Marie Rinkoski [4]. This paper presents a continuation and a further understanding of using Fourier transform infrared spectroscopy to study the quantum behavior of H_2 molecules within the octahedral lattice sites of C_{60}.

The organization of this paper is as follows. Chapter 2 gives background information on the C_{60} molecule and its lattice structure. The characteristics of the potential in an octahedral site are discussed and are important for understanding the translational dynamics of the interstitial hydrogen molecules presented in Chapter 3. In Chapter 3 the vibrational and translational dynamics of an H_2 molecule in an octahedral site are explained to both be that of a simple harmonic oscillator while the rotational dynamics are presented with the rigid rotator model. Even though the molecule is vibrating, not rigid, the rigid rotator model gives a good approximation of the rotational energy levels. With an understanding of the quantized energy levels associated with these dynamics, the discrete energy transitions identified in our absorbance spectra and the selection rules for our system are introduced.

While the size and shape of the octahedral sites in a C_{60} lattice are ideal for trapping hydrogen, as a host lattice it has the large downside of being a highly scattering medium. The result is that we can not use standard transmission spectroscopy to measure the H_2 absorption spectrum because too much of the incident radiation is scattered away from the detector. We instead use a technique of diffuse reflectance whereby the incident infrared radiation is focused onto the C_{60} sample using an ellipsoidal mirror and the unabsorbed and scattered radiation is then collected by another ellipsoidal mirror and focused onto the detector. This technique and the rest of the experimental setup and data collection procedure are described in Chapter 4.

Our experimental results are presented in Chapter 5. This includes absorbance spectra of the H_2 vibrational fundamental and pure rotational transitions, and the vibrational fundamental of D_2 all loaded into a sample of C_{60} powder at a pressure of 1460 psi. While an equivalent spectrum of the H_2 vibrational fundamental has already been published [4], the new data contains an extra peak corresponding to the rotational O, $\Delta J = -2$, transitions which was not identified previously because of overwhelming water absorption lines in the data. The location of this peak in the absorbance spectrum has provided valuable information regarding the frequency shift of the energy transitions from those in gas phase hydrogen.

Chapters 6 contains the analysis and interpretation of our experimental results. Not normally infrared-active, the electric field of the C_{60} molecules surrounding the octahedral sites induces a

dipole moment in the hydrogen molecules enabling them to absorb the incident radiation. The resulting transition peaks in our absorbance spectra all have a constant red-shift from the gas phase of 46 cm^{-1} and an additional shift due to a perturbation of the rotational J levels of -8, 0, or +8 cm^{-1} depending on the transition. The relative intensities of the absorbance peaks in the vibrational fundamental of H_2 are investigated in Chapter 6. A detailed theoretical calculation of these intensities is performed and the results compared with the experimental data show that the Q, $\Delta J = 0$, branches have a much lower relative intensity than the predicted values. We speculate that a possible explanation for this result is the quadrupole moment of the H_2 molecules inducing a dipole moment in the C_{60} molecules.

Lastly, Chapter 7 provides the conclusions of this paper and the future directions of the research. This includes a discussion of the current experimental work being performed with the C_{60} sample loaded with H_2 cooled to liquid helium temperature. A brief description of our preliminary results is given.

Chapter 2

C_{60} Background

The existence of a highly stable molecule consisting of 60 carbon atoms was first proposed by H. W. Kroto, R. E. Smalley, and coworkers as a result of their investigation into the infrared emission of carbon clusters coming from red giant carbon stars. What turned out to be their discovery of C_{60} was begun as an attempt to synthesize carbon clusters that modeled the emission spectra seen by Kroto in these red giant carbon stars using a graphite vaporization technique developed by Smalley and his colleagues [5]. This collaboration between Kroto, Smalley, et al. culminated in a Nature Magazine publication [6] in which, based on the mass spectrum of C_{60}, they proposed the molecular structure of this highly stable molecule to be that of the highly symmetrical truncated icosahedron (see Figure 2.1[1]). Since, this molecular structure of C_{60} has been confirmed through nuclear magnetic resonance (NMR) and infrared (IR) spectrum measurements [5].

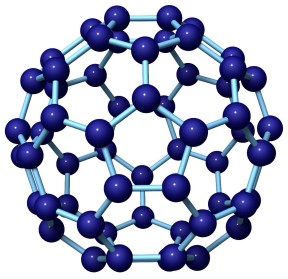

Figure 2.1: C_{60} Molecule

The structure of a truncated icosahedron, made up of only pentagonal and hexagonal faces, is

[1]Image from http://www.surf.nuqe.nagoya-u.ac.jp/nanotubes/omake/fullerenes/fullerenes.html

commonly known because it is the design of a soccer-ball where the black patches form the 12 pentagonal faces and the white patches form the 20 hexagonal faces. This design is translated to the structure of a C_{60} molecule by placing a carbon atom at each of the 60 vertices and a carbon-carbon bond along the seams between each patch. A regular truncated icosahedron has 60 equivalent edges. The "edges" in a C_{60} molecule, however, are a combination of single and double bonds which have respective lengths of 1.46 Å and 1.40 Å as measured by NMR [5]. Therefore, while the molecular structure of C_{60} is that of a truncated icosahedron, it isn't a *regular* truncated icosahedron. The different bonds are arranged such that all the single bonds connect pentagonal and hexagonal faces while the double bonds connect two hexagonal faces. This arrangement has the effect of creating an electronic charge difference between the slightly positive pentagonal faces and the slightly negative hexagonal faces because the pentagons are surrounded by "electron-poor" single bonds while half of the bonds surrounding the hexagons are "electron-rich" double bonds [5].

Due to the rounded, hollow shape of C_{60} it was named buckminsterfullerene, or buckyball for short, after the architect R. Buckminster Fuller who was famous for building geodesic domes. Additional all-carbon molecules with caged molecular structures such as C_{70} and carbon nanotubes are grouped with C_{60} in a class which is referred to as "fullerenes."

At room temperature, C_{60} molecules form a solid with a face-centered cubic (fcc) lattice structure (see Figure 2.2[2]). With a nuclear diameter of 10.34 Å, C_{60} is a relatively large molecule, and because of its size and its nearly-spherical shape, even in its close-packed, solid state there are notable voids between the molecules. There are two types of these interstitial voids: tetrahedral and octahedral

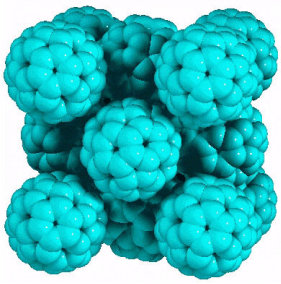

Figure 2.2: C_{60} fcc lattice

sites. There are two tetrahedral sites and one octahedral site per C_{60} molecule. The octahedral

[2]Image from http://rs1.physik.uni-dortmund.de/sem/c60/kap6.htm

sites, which are the larger of the two, have a van der Waals radius of 2.02 Å and are formed by the intersection of six surrounding C_{60} molecules while the smaller, tetrahedral sites, have a van der Waals radius of 1.12 Å and are formed by four C_{60} molecules [5]. With a van der Waals radius of 1.2 Å, H_2 molecules are small enough to be intercalated within the octahedral sites but are too large to fit inside the tetrahedral sites. Neutron diffraction data confirms finite occupancy of the octahedral sites and zero occupancy of the tetrahedral sites [8], and studies of the C_{60}-H_2 loading isotherm support that each octahedral site contains at most one molecule [9]. This system is thus ideal for investigating the quantum dynamics of H_2 molecules because with each molecule trapped in an individually-separated potential well, it represents an almost perfect physical example of the quantum mechanical "particle-in-a-box."

Within an octahedral site, an H_2 molecule will see an overall potential corresponding to the sum of an atom-atom potential between each hydrogen atom and each of the 360 carbon atoms from the six neighboring C_{60} molecules. This atom-atom interaction can be described by a Buckingham potential which is made up of a well known attractive term based on dipole-diople interactions and a less well established repulsive term that is expressed as an exponential decay,

$$V(r) = Be^{-Cr} - \frac{A}{r^6}. \tag{2.1}$$

In this expression, the constants A, B, and C are based on the carbon-hydrogen interaction, and r is their separation. Using values for the constants established by Pertsin and Kitaisordsky [10] of $A = 5.941 \text{ eV} \cdot \text{Å}^6$, $B = 678.2$ eV, and $C = 3.67 \text{ Å}^{-1}$ [8], Scott Forth wrote a Mathematica program to find the total potential within an octahedral site with the summation expression

$$V_{total}(r) = \sum_{i=1}^{2} \sum_{j=1}^{360} Be^{-Cr_{ij}} - \frac{A}{r_{ij}^6}, \tag{2.2}$$

where r_{ij} is the separation of the ith hydrogen atom from the jth carbon atom [11]. He found that for displacements from the center of the site up to 0.5 Å, the potential is approximately that of a simple harmonic oscillator. Additionally, it has also been shown that the potential of an octahedral site is nearly spherically symmetric; that the change in potential seen by an H_2 molecule as a function of its orientation within the site is only about 1.8% [8]. Thus, a spherical simple harmonic oscillator provides a reasonable model for the potential within an octahedral site.

As previously mentioned, at room temperature $\approx$ 295 K, solid C_{60} forms an fcc lattice. NMR measurements have shown that at this temperature the molecules are randomly oriented and freely

rotating in their lattice positions with a period of about 10^{-11} s [5]. This rotation would allow us to ignore the regions of positive and negative charge on a C_{60} molecule and treat them as neutral spheres as long as we probe the system at a time-scale much longer than their rotational period. Unfortunately, experimental results presented in Chapter 5 suggest that our probe is on a comparable time-scale to this rate of rotation. At 261 K, C_{60} goes through a phase transition and molecules below this temperature no longer rotate freely. Instead, they become orientationally ordered in a $Pa\bar{3}$ structure and have a rapid racheting motion between symmetrically equivalent orientations [4]. In this phase, with the C_{60} molecules in a $Pa\bar{3}$ orientation, the octahedral sites have inversion symmetry. These changes in the C_{60} lattice are important when considering the low temperature dynamics of intercalated H_2.

Chapter 3

Quantum Dynamics

3.1 Vibrational Dynamics

We start by picturing the vibrational dynamics of our hydrogen molecule with the classical "dumbbell" model of two identical masses connected by a spring. In this case, the motion of the atoms

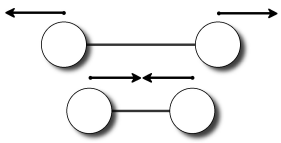

Figure 3.1: Molecular vibration

is that of a simple harmonic oscillator where they alternate between moving toward and away from each other as depicted in Figure 3.1. For the simple harmonic motion of a single mass, m, on a spring we know that by using Hooke's Law,

$$F = -kx \tag{3.1}$$

where x is the distance from equilibrium and k is the spring constant, we find a solution for the frequency of oscillation given by

$$\nu = \frac{1}{2\pi}\sqrt{\frac{k}{m}}. \tag{3.2}$$

The corresponding frequency of oscillation for a dumbbell system is identical except that m is replaced by the reduced mass, μ. Relating this model to a diatomic hydrogen molecule, the spring constant, k, represents the "spring" characteristic of the chemical bond and, since it is made up of two identical atoms, the reduced mass is simply equal to $\frac{1}{2}m$ with m being the mass of a single hydrogen atom.

Making these substitutions in Equation (3.2), the fundamental vibrational frequency of H_2 is

$$\nu_o = \frac{1}{2\pi}\sqrt{\frac{2k}{m}}. \tag{3.3}$$

This frequency has an accepted value of 4161 cm^{-1} for free hydrogen [12]. (All frequencies in this paper will be given in wavenumbers, cm^{-1}, which is determined by $\frac{1}{\lambda}$, where λ is the wavelength in cm.)

The dumbbell model of a hydrogen molecule can only be taken so far because classical approximations are only reasonable when the thermal energy is much greater than the quantized energy level separation, or when there is significant thermal population of excited energy levels. From Equation (3.1) we derive the potential energy of a simple harmonic oscillator to be

$$V = 2\pi^2 m\nu_o^2 x^2. \tag{3.4}$$

Using this equation for the potential and solving the time-independent Schrödinger equation we find that the quantized energies of oscillation, or the vibrational energies, of our H_2 molecule are

$$E_{vib} = \left(\nu + \frac{1}{2}\right)\nu_o. \tag{3.5}$$

In this expression, ν is the vibrational quantum number and has values of 0, 1, 2... It is clear from this equation that the vibrational energy levels will have an equal spacing of ν_o. At room temperature $T \approx 295$ K and, in equivalent units, $\nu_o \approx 5950$ K. Thus it is unreasonable to use a classical approximation for the vibrational dynamics of H_2.

Deuterium, D_2, is an isotope of hydrogen and thus identical to H_2 expect that each nucleus contains a neutron. Since the mass of a neutron is nearly the same as the mass of a proton, D_2 has approximately twice the mass of H_2. Otherwise identical to hydrogen, we can easily derive the vibrational dynamics of D_2. The chemical bond between the atoms has not changed so k, the "spring constant," should be the same and so simply replacing $2m$ for m in Equation (3.3) we find

$$\nu_o(D_2) = \frac{1}{2\pi}\sqrt{\frac{k}{m}} = \frac{\nu_o(H_2)}{\sqrt{2}}. \tag{3.6}$$

This formula gives the fundamental vibrational frequency of D_2 as 2942 cm^{-1} which is only off by about 1.7% from the accepted value of 2994 cm^{-1}. This slight discrepancy is a result of anharmonicity in the vibrational motion. Using this value for ν_o we can find the vibrational energies of D_2 with Equation (3.5). While in this example our approximation from the H_2 case is not necessary because we know the exact value for D_2, we use this tactic extensively in Chapter 6 for developing a fit to the D_2 spectral data from our H_2 fit.

3.2 Rotational Dynamics

In addition to vibrating as a simple harmonic oscillator, diatomic molecules have rotational dynamics as pictured classically in Figure 3.2, and the energies associated with this rotation will also be quantized. Beginning again with the dumbbell model, we ignore the vibrational motion of the

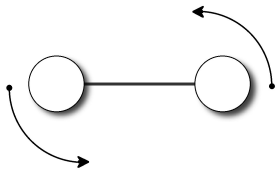

Figure 3.2: Molecular rotation

molecule and assume that the two hydrogen atoms are connected by a massless, rigid rod. This is called the rigid rotator model. The classical energy of such a system is given by

$$E = \frac{L^2}{2I}, \tag{3.7}$$

where L is the angular momentum and $I = \mu r^2$ is the moment of inertia about the axis of rotation with r being the separation of the two masses. Again, we must analyze the system in the quantum rather than the classical regime. To find the quantized rotational energies we use $\frac{L^2}{2I}$ as the hamiltonian and substitute into the time-independent Schrödinger equation:

$$H\psi = E\psi \Rightarrow \frac{L^2}{2I}\psi = E\psi. \tag{3.8}$$

Knowing that ψ is an eigenfunction of L^2 with eigenvalues $\hbar^2 J(J+1)$ where J has integer values 0, 1, 2..., we conclude that the rotational energies are

$$E_{rot} = \frac{\hbar^2 J(J+1)}{2I}, \tag{3.9}$$

where J is the rotational quantum number. This expression is commonly written in the form

$$E_{rot} = B_\nu J(J+1), \tag{3.10}$$

where B_ν is the rotational constant of the molecule. The term "constant" is misleading, because B_ν varies slightly from the vibrational ground state ($\nu = 0$) to the vibrational excited states ($\nu = 1, 2, 3\ldots$). For H_2, $B_0 = 59.3$ cm^{-1} and $B_1 = 56.4$ cm^{-1}, while for D_2, $B_0 = 29.9$ cm^{-1} and $B_1 = 28.8$ cm^{-1} [13]. Substituting these values into Equation (3.10) we see that the rotational energy levels of H_2 are on the order of a few hundred wavenumbers.

Unfortunately, because H_2 molecules are vibrating, the rigid rotator model doesn't produce the exact energies for our system. We should actually view the molecule as a rotating oscillator, because the vibration of the molecule perturbs the rotational energies. This perturbation is small because the difference between the vibrational and rotational energies is large ($\backsim$4000 cm^{-1} vs. a few hundred cm^{-1}) [14]. For heaver molecules the perturbation is barely detectable because $E_{vib} \propto \sqrt{\frac{1}{\mu}}$ while $E_{rot} \propto \frac{1}{\mu}$ so as the mass increases, the difference between the vibrational and rotational energies increases, and therefore the perturbation decreases. The problem of the rotating oscillator has been worked out, and the quantized energy levels were found to be

$$E_{rot,\nu} = B_\nu J(J+1) - D_\nu[J(J+1)]^2 + H_\nu[J(J+1)]^3 + L_\nu[J(J+1)]^4 + \ldots \tag{3.11}$$

The additional coefficients D_ν, H_ν and L_ν have values of 0.046 cm^{-1}, 4.9×10^{-5} cm^{-1}, and -6.1×10^{-8} cm^{-1} for hydrogen in its vibrational ground state [15, 12]. The small effect of the perturbation is clear from the rapid decrease in magnitude of the coefficients with each successive term of Equation (3.11). When creating fits to the experimental results in Chapter 6, we use experimentally determined values of the rotational energies of free H_2 for determining the center frequencies of the rotational peaks, but for the intensity calculations we use the energies from the rigid rotator model because the difference from the literature values is within our experimental error.

3.3 Translation Dynamics

Unlike free hydrogen, the H_2 molecules trapped within the octahedral sites of C_{60} have quantized translational motion (Figure 3.3). As mentioned in Chapter 2, the potential of an octahedral site

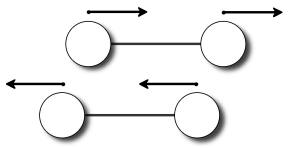

Figure 3.3: Molecule translation

is approximately that of a spherical simple harmonic oscillator for displacements of less than 0.5 Å. Therefore, the translational energies are approximately that of a three-dimensional harmonic oscillator:

$$E_{trans} = \left(n + \frac{3}{2}\right) n_o, \tag{3.12}$$

where n is the translational quantum number. Experimental results suggest a value for n_o of about 127 cm^{-1} [4]. The temperature equivalent of this energy is $n_o \approx 181$ K, which implies that, unlike the

vibrational case, there should be significant thermal population in the translational energy levels at room temperature. Thus we can make at least a crude estimation of the translational energy at room temperature using the Equipartition Theorem. This theorem says that for each degree of freedom in the system there is an associated energy of $\frac{1}{2}kT$. The translation motion of an H_2 molecule has three degrees of freedom and so an energy of $\frac{3}{2}kT$. Adding this to the zero-point or the ground state energy, we have an estimate for the translational energy at room temperature as

$$E_{trans}(T = 295 \text{ K}) \approx \frac{3}{2}kT + \frac{3}{2}n_o. \tag{3.13}$$

When $T = 295$ K, $\frac{3}{2}kT \approx 38$ meV. Using $n_o = 127$ cm^{-1}, the zero-point translational energy is about 24 meV. Thus from very low temperature (only the zero-point energy) to room temperature (the zero-point energy plus the thermal energy) the translational energy increases by about a factor of 2.6. The mean-square amplitude of displacement, $\langle R^2 \rangle$, for an H_2 molecule in a C_{60} lattice octahedral site at very low temperature (4.2 K) has been estimated as 0.2 Å^2 [8]. In simple harmonic motion, $E \propto R^2$ so we can argue that since the energy will approximately increase by a factor of 2.6 from 4.2 K to 295 K, $\langle R^2 \rangle$ will go up by about 2.6. Finally, making the assumption that $\langle R \rangle = \sqrt{\langle R^2 \rangle}$, we very crudely estimate the displacement of an H_2 molecule at room temperature as $\sqrt{0.2 \text{ Å}^2 \times 2.6} \approx 0.7$ Å. Thus it is a reasonable approximation to describe the total potential in an octahedral site by a spherical simple harmonic oscillator, but there will be some anharmonicity in the translational energy levels due to the potential not being simple harmonic for displacements larger than 0.5 Å.

3.4 IR Spectroscopy and Allowed Transitions

IR spectroscopy allows us to probe the vibrational, rotational and translational dynamics of the H_2 molecules based on the frequencies of radiation absorbed by the system. Since molecules can only posses energies at discrete values, they are only able to absorb photons with precise frequencies, ν, related to the difference between two energy levels through the expression

$$\Delta E = h\nu, \tag{3.14}$$

where h is Planck's constant. By absorbing light at these frequencies a molecule will be excited to a higher energy level. However, molecules are only IR active, meaning able to absorb infrared radiation, if they have a dipole moment, μ [16]. From electrodynamics we know that if a molecule has a permanent dipole moment, then its vibrational, rotational, and translational dynamics will result in an oscillating dipole moment which acts as an antenna to absorb or emit radiation at its

precise frequencies of oscillation [17].

In addition, for a transition to occur there must be a change in the oscillating dipole moment from the initial to the final state of the molecule. This means that if the matrix element of the dipole moment between two states, ψ_a and ψ_b, is zero, then the transition between those states is forbidden. In other words, a transition is allowed only if

$$\langle \psi_a \mid \mu \mid \psi_b \rangle \neq 0, \tag{3.15}$$

where μ is the dipole moment and the states ψ_a and ψ_b have associated vibrational, rotational, magentic, and translational quantum numbers ν, J, m, n, and ν', J', m', n' respectively [18].

H_2 is a symmetric, diatomic molecule so it doesn't have an intrinsic dipole moment because, due to symmetry, there is an equal sharing of the electrons [16]. Since it has no dipole moment H_2 is not visible with infrared spectroscopy under normal conditions, but when intercalated within C_{60}, H_2 molecules obtain an induced dipole moment due to the electric field of the C_{60}. The magnitude of the induced dipole moment is given by

$$|\mu_{ind}| = \alpha |E_{C_{60}}|, \tag{3.16}$$

where α is the polarizability of H_2 and $E_{C_{60}}$ is the electric field due to the C_{60} molecules surrounding an octahedral site [18]. These sites have inversion symmetry so the electric field will be zero at the center, and this implies that in a classical picture, an H_2 molecule located at the center will have no dipole moment. If the potential due to the C_{60} molecules goes as a spherical simple harmonic oscillator, then it can be written in the form

$$\vec{V}_{C_{60}} = \frac{1}{2} A \vec{R}^2, \tag{3.17}$$

where A is a constant and $\vec{R}$ is the displacement vector of the center of mass of an H_2 molecule from the center of the site. Thus

$$\vec{E}_{C_{60}} = -\nabla \vec{V}_{C_{60}} = -A\vec{R}, \tag{3.18}$$

and therefore from Equation (3.16), the magnitude of the induced dipole moment will increase linearly with R.

We can derive the selection rule for translational, Δn, transitions using this fact that μ_{ind} changes linearly with R. Since R is related only to the translational motion of the H_2 molecule, knowing that

we need $\langle \psi_a \mid \mu \mid \psi_b \rangle \neq 0$, implies that the n quantum numbers of the initial and final states must satisfy $\langle n \mid R \mid n' \rangle \neq 0$. Analogous to the one-dimensional case where the selection rule is obvious when R is rewritten as a ladder operator, we find from this requirement that Δn must be equal to ± 1 [19].

That μ_{ind} is also linearly dependent on the polarizability, α, gives insight into the vibrational, $\Delta\nu$, transitions because α is itself a function of the H_2 internuclear separation which is in turn related to the vibrational motion of the molecule. Thus we have that for a transition to occur, the vibrational quantum numbers must satisfy $\langle \nu \mid \alpha \mid \nu' \rangle \neq 0$. Performing a Taylor expansion about the equilibrium internuclear separation we find

$$\alpha(\rho) = \alpha_o + \frac{\partial \alpha}{\partial \rho}\rho + \frac{\partial^2 \alpha}{\partial \rho^2}\rho^2 + \ldots, \tag{3.19}$$

where ρ is the difference in the internuclear separation from the equilibrium position [19]. Written in this way, the first term corresponds to the pure rotational, $\Delta\nu = 0$, transition, the second term corresponds to the vibrational fundamental with $\Delta\nu = 1$, and the third term corresponds to the vibrational overtone with $\Delta\nu = 2$.

The rotational J quantum numbers represent the quantized units of angular momentum of the molecule. Since angular momentum must be conserved and photons carry one unit of angular momentum, it seems that the selection rule for rotational transitions should be $\Delta J = \pm 1$. In actuality the selection rule for our system is $\Delta J = 0, \pm 2$ because as the H_2 molecule oscillates in the octahedral site, it sees an oscillating electric field from the C_{60} molecules and this acts as a second "photon" with another unit of angular momentum. Our system therefore has a rotational selection rule associated with the two photon Raman effect rather than standard IR spectroscopy [24]. A more rigorous derivation of this selection rule is presented in Chapter 6. A summary of the selection rules is given in the table below.

Summary of Selection Rules		
Translational	$\Delta n =$	$\pm 1, 0$[1]
Rotational	$\Delta J =$	$\pm 2, 0$
Vibrational	$\Delta \nu =$	$0 \Rightarrow$ Pure Rotational
		$1 \Rightarrow$ Fundamental
		$2 \Rightarrow$ Overtone

Because writing out the change in each of the quantum numbers to describe a given transition can be tedious, a shorthand has been established where the letters S, R, Q, P, and O represent changes of $+2, +1, 0, -1$, and -2 [18]. For example, we write a $\Delta J = +2, \Delta n = +1$ transition as $S_R(0)$. The first letter refers to the ΔJ rotational transition, the subscript (which is occasionally left off) refers to the Δn translational transition, and the number in brackets is the inital J quantum number. The

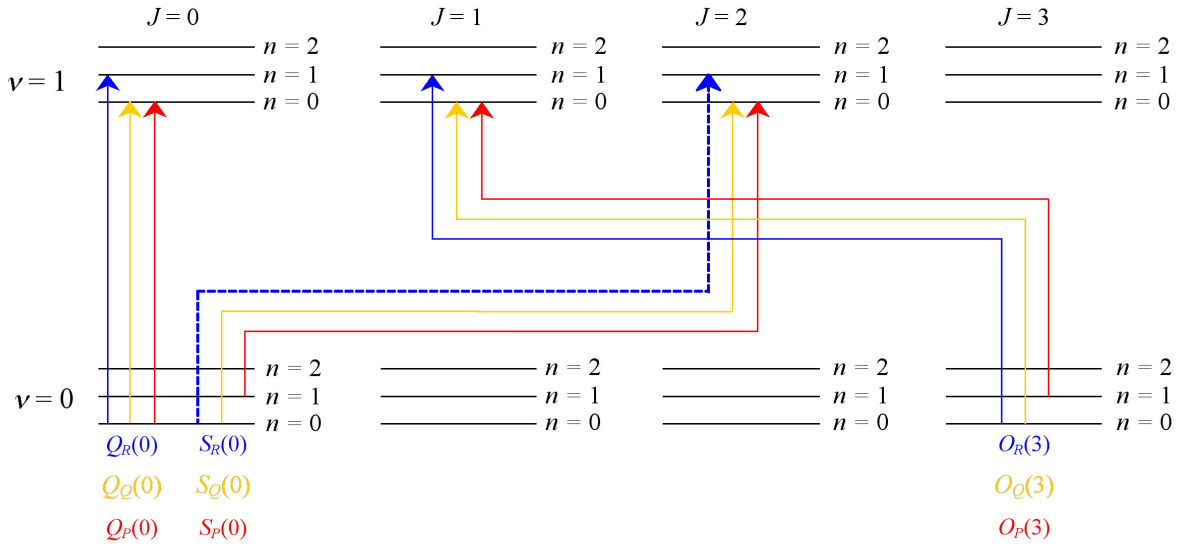

Figure 3.4: Selected allowed transitions of the vibrational fundamental. The red, yellow, and blue lines are the translational P, Q, and R transitions. The dashed blue line is the $S_R(0)$ transition. The energy associated with this specific transition is given in Equation (3.20).

$S_R(0)$ transition of the vibrational fundamental is shown by the dotted blue line in Figure 3.4 which displays a few other allowed transitions. This transition represents an H_2 molecule absorbing a single photon with the precise energy,

$$\begin{aligned} E_{photon} &= E_{vib(\nu=1)} + E_{rot(J=2)} + E_{trans(n=i+1)} \\ &\quad -[E_{vib(\nu=0)} + E_{rot(J=0)} + E_{trans(n=i)}]. \end{aligned} \tag{3.20}$$

Additionally, we can quickly see that there will be no $O(0)$ or $O(1)$ transitions, because the O transitions have $\Delta J = -2$. The first allowed transition will be $O(2)$ which begins in the $J = 2$ state and ends in the rotational ground state.

[1] As will be explained in Chapter 5, it turns out that $\Delta n = 0$ is also an allowed transition.

It is important to note that for any transition to occur, the change in each quantum number must satisfy its corresponding selection rule. For example, it would seem at first that we should see a peak in our absorbance spectra corresponding to the $S_Q(1)$ transition which would correspond to the molecule absorbing a photon of energy

$$\begin{aligned} E_{photon} &= E_{vib(\nu=1)} + E_{rot(J=3)} + E_{trans(n=i)} \\ &\quad -[E_{vib(\nu=0)} + E_{rot(J=1)} + E_{trans(n=i)}] \end{aligned} \tag{3.21}$$

or

$$E_{photon} = E_{vib(\nu=1)} + E_{rot(J=3)} - [E_{vib(\nu=0)} + E_{rot(J=1)}], \tag{3.22}$$

but in actuality this transition shouldn't be allowed because $\langle n \mid R \mid n' \rangle = 0$ and therefore $\langle \psi_a \mid \mu \mid \psi_b \rangle = 0$. This relates to the classical picture of the H_2 molecule sitting at the center of an octahedral site where $E_{C_{60}} = 0$ and so it has no μ_{ind} and therefore can't interact with the incident radiation.

Chapter 4

Experimental Technique

4.1 Equipment

The spectral data to be analyzed in this paper were taken with a Bomem DA3 Fourier Transform Infrared (FT-IR) Spectrometer. The basic design of this spectrometer is that of a standard Michelson interferometer. Developed by Michelson near the end of the 19^{th} century, the interferometer uses the wave-like properties of light to determine with great accuracy the wavelength of an incoming monochromatic light source [20]. A schematic of a standard Michelson interferometer is shown in Figure 4.1. It contains a light source incident on a beamsplitter set at a 45° angle; two mirrors, one

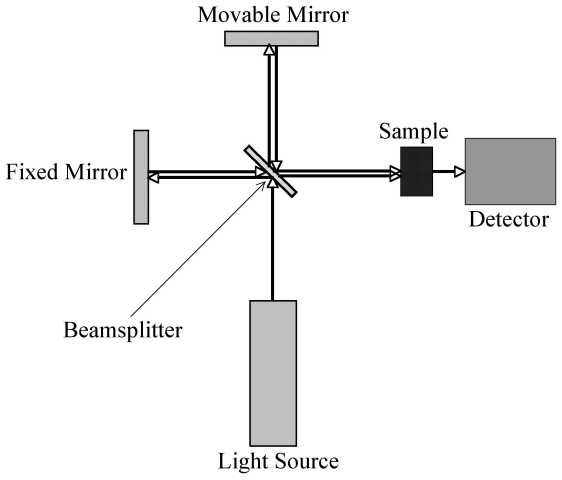

Figure 4.1: Schematic of a Michelson Interferometer

of which is movable and the other of which is fixed, set at 90° to each other; and a detector. When using the interferometer to gain insight to the absorbance spectrum of a sample, the sample is placed

in the path of the beam directly before the detector. In our spectrometer, we used an infrared globar source, a potassium bromide (KBr) beamsplitter, and a liquid nitrogen (LN_2) cooled MCT detector.

The beamsplitter in an interferometer is designed to have optical properties such that it transmits half of the incident beam toward the movable mirror and reflects the other half of the beam toward the fixed mirror. When the displacement of the movable mirror from the beamsplitter is not equal to the displacement of the fixed mirror, the beam that reflects off it will have a different path length giving it a phase difference from the other beam. When the two beams recombine along the path to the detector, this phase difference will cause them to interfere. As the mirror moves back and forth, the detector will see intensity fringes as there is constructive (the path difference is an integer multiple of λ) and destructive (the path difference is a half-integer multiple of λ) interference. If the light source is monochromatic, then a plot of the intensity received by the detector against the path length difference will be a cosine curve with a frequency equal to that of the light source [see row a. of Figure 4.2[1]]. This kind of plot is called an interferogram.

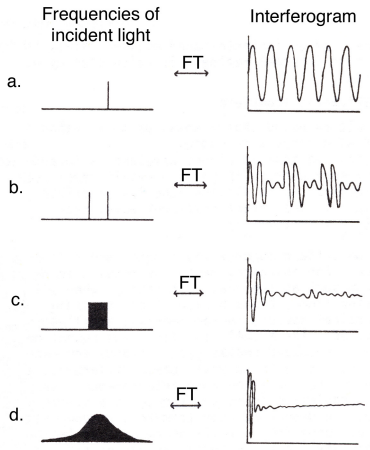

Figure 4.2: Sample interferograms for: a. monochromatic radiation; b. two frequencies; c. a narrow band of frequencies with constant amplitude; d. a broad band of frequencies with varying amplitudes.

Figure 4.2 also shows the interferograms for multiple frequency light sources. All of these have a large peak at zero path difference because in this situation all frequencies of light will constructively interfere with themselves. To determine the precise frequencies that make up a source of polychormatic radiation, the mathematical technique of a Fourier transform is used in combination with an interferometer. This is the technique used in our experimental set-up. Our detector records the

[1]Image adapted from T. Theophanides, page 37.

intensity of the incident light and converts it into a voltage. This voltage plotted against the path difference then creates our interferogram. We use BOMEM's PDCA data acquisition software to acquire this interferogram and convert it into a conventional spectrum using the Fourier transform equation:

$$B(\nu) = \int_{-\infty}^{+\infty} I(\delta)\cos(2\pi\nu\delta)d\delta. \tag{4.1}$$

A conventional spectrum is simply the plot of the spectral power density, B, versus frequency. $I(\delta)$, the intensity at the detector as a function of the difference in path length, δ, represents the interferogram [20]. The reverse procedure to find $I(\delta)$ from $B(\nu)$ can be performed using

$$I(\delta) = \int_{0}^{+\infty} B(\nu)\cos(2\pi\nu\delta)d\delta. \tag{4.2}$$

Finally, a conventional spectrum is converted into a spectrum of just the hydrogen absorbance though techniques described in the Data Manipulation section.

Since H_2 is not normally IR-active, the absorption seen in our spectra is only a result of interaction with the C_{60} host lattice, and thus the absorption intensity is quite low. In addition, C_{60} is highly scattering, so we can't use standard transmission spectroscopy because very little of the incident beam would make it to the detector, severely diminishing our already weak signal. We instead use diffuse reflectance spectroscopy (DRIFTS). In this technique, the incoming beam is focused onto the sample via an ellipsoidal mirror and then the radiation that is diffusely reflected from the sample is collected by another ellipsoidal mirror and focused onto the detector. A schematic of our DRIFTS rig, made by the Spectra-Tech Corporation, is shown in Figure 4.3. DRIFTS is a common technique

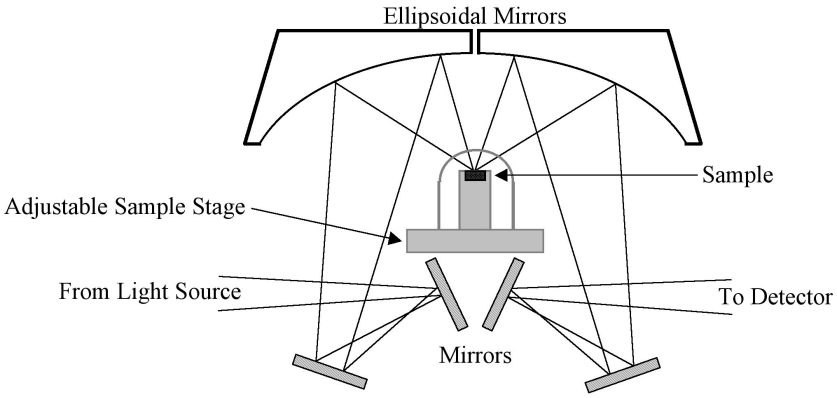

Figure 4.3: Schematic of a DRIFTS rig

for performing spectroscopic measurements on powdered samples because the samples don't have to

be pressed into a pellet as they would need to be in order to perform transmission measurements [21]. More importantly, however, DRIFTS has great applications for the study of absorbed molecules because it is possible to enclose the sample in a chamber where its atmosphere can be altered even though the rest of the spectrometer must be evacuated during normal operating conditions [22]. In our case, by enclosing the sample in a dome we are able to load hydrogen into the sample in-situ, thus not disturbing the C_{60} powder. The dome we use to enclose the sample has a steel frame with zinc selenide (ZnSe) windows which are transparent in the IR from approximately 20,000 - 454 cm^{-1} and can withstand pressures up to 1500 psi.

4.2 Procedure

A detailed account of the standard procedure for acquiring spectra can be found in Appendix B of Scott Forth's honors thesis [11]. Here I will give a general overview of the process with specific details only of the steps that differ from Scott's description.

The first step in preparing the system is to pump out the MCT detector. We discovered that over time its vacuum deteriorates so that when cooled with LN_2, the window on the bottom of the detector becomes slightly cooled causing water molecules from the air to condense on it. Water is highly IR-active and absorption due to the presence of these water molecules can cause peaks in our spectra that overpower the weak absorption peaks of the hydrogen molecules. By using a diffusion pump for about four hours to pump out the vacuum of the detector, the water absorption lines in our spectra are greatly diminished. This procedure should be performed every few weeks to maintain a good vacuum.

The next step is to load the C_{60} sample into the pedestal of the DRIFTS rig (see Figure 4.3). The C_{60} powder we used was purchased from the MER Corporation and rated to a purity of 99.9%. After the sample is loaded, the spectrometer and the computer interface must be prepared. This involves turning on the cooling water and the spectrometer (without the cooling water the light sources may overheat and become damaged), loading the KBr beamsplitter, aligning the spectrometer, and establishing a connection between the spectrometer and the computer. The last steps before the entire system is evacuated and ready to acquire spectra are to adjust the sample height and attach the ZnSe dome over the sample pedestal. Because an elliptical mirror is used to focus the beam in the DRIFTS rig, the strength of the signal reaching the detector is very sensitive to the height of the

sample. This height is finely adjusted using an Alan key and then the dome is screwed in place over the sample. Once this is completed the spectrometer is evacuated and when the pressure is below 1.0 Torr, the system is ready to take spectra.

We first take a number of spectra of the pure C_{60} sample to establish a background reference and assure that the system is functioning properly. For these spectra we normally take between 200 and 1000 scans, where a single scan corresponds to the movable mirror going through one cycle. After establishing a good background, pure hydrogen gas is introduced into the dome to a desired pressure through a gas handling setup (see [11] for a detailed description of this apparatus). Since the loading isotherm for the hydrogen follows a logarithmic dependence with time [9], we initially see a large change in the H_2 absorption peaks in our spectra and over time the rate of growth of these peaks slows down. At room temperature with C_{60} powder, we usually see no detectable change in the absorption about two hours after introducing the hydrogen. At this point we take long spectra (a few thousand scans), and we are ready to prepare the data for analysis through the manipulations described below. If instead of using a C_{60} powder we use large single crystals of C_{60}, the time for the sample to become fully loaded with H_2 is much longer.

4.3 Data Manipulation

When a photon of frequency ν is absorbed by H_2 molecules in the system, it reduces the intensity of the incident beam at that frequency causing a dip in the raw spectrum. In order to create a spectrum of just the H_2 absorption we must reference this spectrum to one taken under identical circumstances but without the hydrogen present. Then we can conclude that the additional absorption dips with the hydrogen loaded are due solely to its absorption and and not other factors such as the absorbance of the C_{60}. There are two standard techniques for referencing to background spectra: transmission and absorbance. Transmission is the direct ratio of the intensity of the loaded sample (C_{60} plus H_2), I, to the intensity of the unloaded sample (pure C_{60}), I_0:

$$Tra = \frac{I}{I_0}. \tag{4.3}$$

The equation for absorbance is given by the negative log of the transmission:

$$Abs = -\log\left(\frac{I}{I_0}\right). \tag{4.4}$$

All spectra given in this paper we produced using absorbance. However, we found that we are able to get a cleaner spectrum of the H_2 absorption peaks if we reference not to a spectrum of pure C_{60}, but

to the first spectrum taken after the hydrogen gas is introduced. When this is done, we diminish the appearance of a large, broad peak throughout the spectrum coming from absorption of the hydrogen gas which remains in the dome but not absorbed by the C_{60}. This unabsorbed hydrogen gas is visible in the IR because at high pressure it has collision-induced absorption whereby the molecules colliding into one another induce dipole moments which interact with the incoming radiation [23]. By taking an absorbance spectrum of KBr powder (in which H_2 will not become intercalated) with hydrogen gas loaded at 1000 psi, it was found that the intensity of the collision-induced absorption is about one tenth as strong and much broader than the absorption of H_2 molecules intercalated in the C_{60} [11].

In order to reduce the noise in our final spectrum we average together as many spectra with as many scans as possible using the BOMEM Grams software. Once we have created the cleanest possible absorption spectra we often need to manipulate the results with a baseline correction. Since much time elapses (approximately 2 hours) between the acquisition of the background reference and the final, fully loaded, spectra we often see a significant change in the baseline of the raw spectra due to the system drifting overtime. The result is that our absorption spectrum will have a steep, sloping baseline. We correct for this sloping baseline using the 'baseline' function in the Grams software.

Chapter 5

Experimental Results

Figure 5.1[1] shows the absorption spectrum obtained for H_2 within the octahedral sites of a C_{60} lattice with our assignment of the peaks. This spectrum was created by averaging together 1400 scans

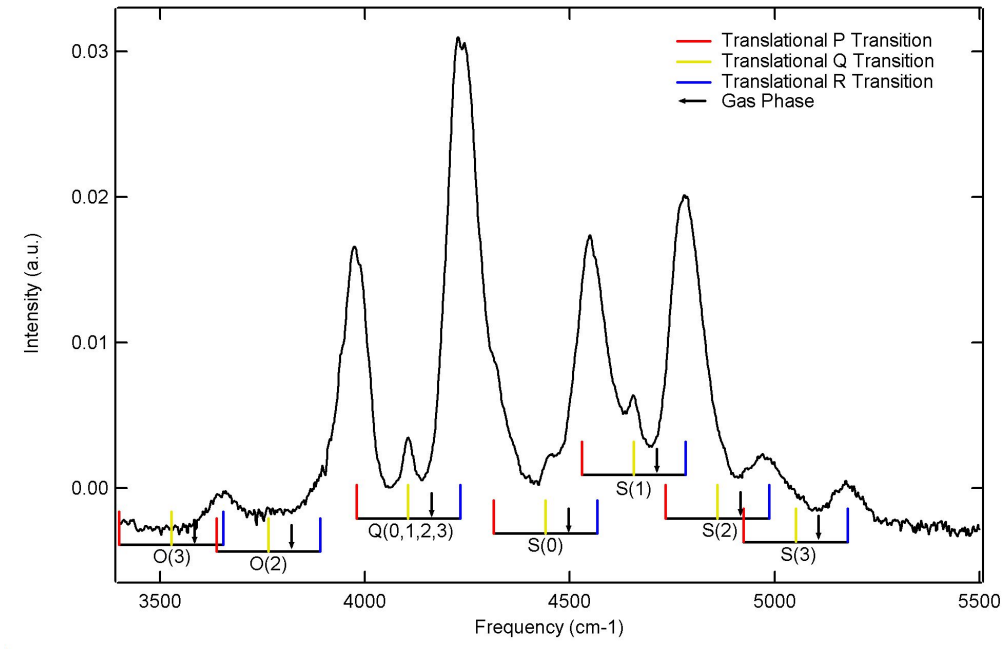

Figure 5.1: Data of the H_2 vibrational fundamental taken with the high sensitivity MCT detector

with a resolution of 4 cm^{-1} taken at room temperature with a high sensitivity LN_2 cooled MCT detector. The scans were taken approximately an hour an a half after the hydrogen gas was initially introduced into the system at a pressure of 1460 psi. The averaged raw spectrum was turned into the above absorbance spectrum not by referencing to a spectrum of pure C_{60} but to a spectrum taken

[1]The data in this Figure was taken on December 3, 2004. It is an average of files 43-45 referenced to 15.

two minutes after the H_2 was added.

The above spectrum shows the transitions associated with the vibrational fundamental ($\Delta\nu = 1$). The large Q branch in the spectrum, which is a combination of the $Q(0)$, $Q(1)$, $Q(2)$, and $Q(3)$ branches, represents the hydrogen pure vibrational transitions ($\Delta J = 0$). The other $S(0)$, $S(1)$, $S(2)$, $S(3)$, $O(2)$, and $O(3)$ branches represent the rotational-vibrational transitions ($\Delta J = +2$ or -2). Each branch is made up of three peaks. The center Q peaks (labeled in yellow) correspond to pure vibrational or pure rotational-vibrational transitions ($\Delta n = 0$) while the P and R peaks (red and blue) correspond to the translational sidebands ($\Delta n = -1$ and $\Delta n = +1$ respectively). These translational sidebands are symmetrically located at ± 127 cm^{-1} from the center Q peaks for all of the branches displayed in the Figure.

The black arrows in Figure 5.1 mark the transitional frequencies for gas phase hydrogen which are related to the center Q peaks because hydrogen molecules in the gas phase don't have quantized translational motion. Comparing the arrows and the yellow Q peaks we see that there is a small shift that is relatively consistent for all of the branches. This is the first spectrum to show the O branches which were previously hidden due to overwhelming water absorption lines at that frequency. It was previously thought that all of the rotational branches were red-shifted by an equal amount of 54 cm^{-1} [4], but we have since found a better fit to this data with shifts of 46, 54 and 38 cm^{-1} for the Q, S and O branches. This implies that while the hydrogen molecules are almost freely rotating in the octahedral sites, there is a slight perturbation in the rotational energy levels. These shifts are analyzed in Chapter 6.

One surprising thing about this data is the clear existence of the center Q peaks for the different branches. While their intensities are decreased significantly from the P and the R peaks, they are still evident. As discussed in Chapter 3, we didn't expect to see these peaks because they correspond to a forbidden transition of $\Delta n = 0$, or the classical picture of the H_2 molecule sitting in the center of the potential well where $E_{C_{60}}$ is zero. We speculate that we do see these peaks because the electric field at the center of the octahedral site isn't exactly zero because there isn't perfect inversion symmetry so the electric field from the C_{60} molecules doesn't perfectly cancel out. That there is perfect inversion symmetry in the octahedral sites depends on the assumption that the C_{60} molecules can be treated as uniformly charged spheres such that their relative orientations don't effect the overall

potential. As mentioned in Chapter 2, however, they are *not* uniformly charged; the pentagonal and hexagonal faces have slightly positive and negative charges. Above the 261 K phase transition, the C_{60} molecules are nearly freely rotating with a frequency of about 10^{11} Hz. Our "probe," however, is the H_2 molecule which is translating back and forth at a frequency of 127 cm^{-1} or about 4 $\times 10^{12}$ Hz. Thus the potential that it "sees" at any given moment may not have inversion symmetry because in a "snapshot" the C_{60} molecules are randomly oriented. Below the phase transition, when the C_{60} molecules are ordered in a $Pa\bar{3}$ structure, the octahedral sites do have inversion symmetry. Instead of rotating randomly, they rachet between symmetrically equivalent orientations maintaining the inversion symmetry. Thus below the phase transition there should be more inversion symmetry and so less electric field at the center of the site thus less allowed $\Delta n = 0$ transitions. Indeed experimental data taken with our sample below 261 K shows the center Q peaks nearly disappear [11].

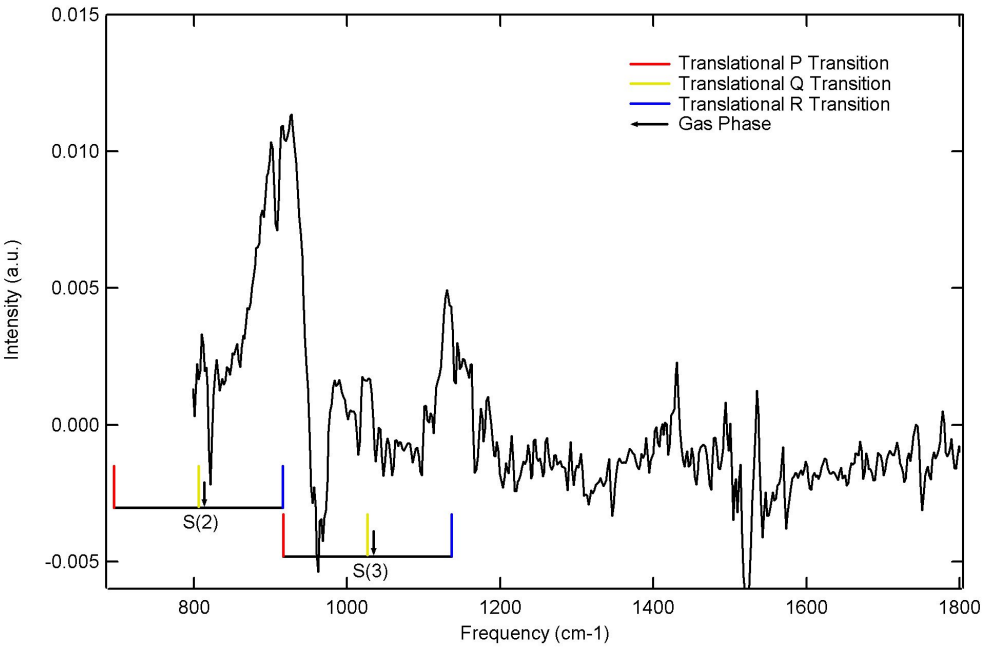

Figure 5.2: Pure rotational data of H_2 taken with the high sensitivity MCT detector

While taking data of the H_2 vibrational fundamental with the high sensitivity MCT detector, we discovered two peaks at the low frequency end of the spectrum which also appeared once the hydrogen was added to the system. After analyzing the positioning of these peaks we determined that they are some of the peaks associated with the pure rotational, $\Delta\nu = 0$, transition. Figure 5.2[2]

[2]This spectrum is made from the same files as those used in Figure 5.1.

shows this low frequency data of the pure rotational peaks with our assignment of the branches.

The pure rotational data in Figure 5.2 was taken from the same spectrum as the vibrational fundamental data in Figure 5.1. Even though the intensities of the these peaks are much larger than that of the $S_R(2)$ or $S_R(3)$ in the fundamental, they are harder to resolve because the noise is much worse. The increased noise is due to two factors working against us in this frequency range; first, the detector is at the very edge of its functional range and second, the C_{60} host is absorbing. The spectrum of the pure rotation data in Figure 5.2 stops at 800 cm^{-1} because below this point the detector dies completely and the spectrum is only noise. Thus we are unable to see the rest of the peaks associated with the pure rotational transitions because they are all at lower frequencies. The other big problem is the absorption the C_{60}. An absorbance spectrum of pure C_{60} is shown in Figure 5.3. This spectrum was created by referencing a raw spectrum of C_{60} to one taken of pure KBr

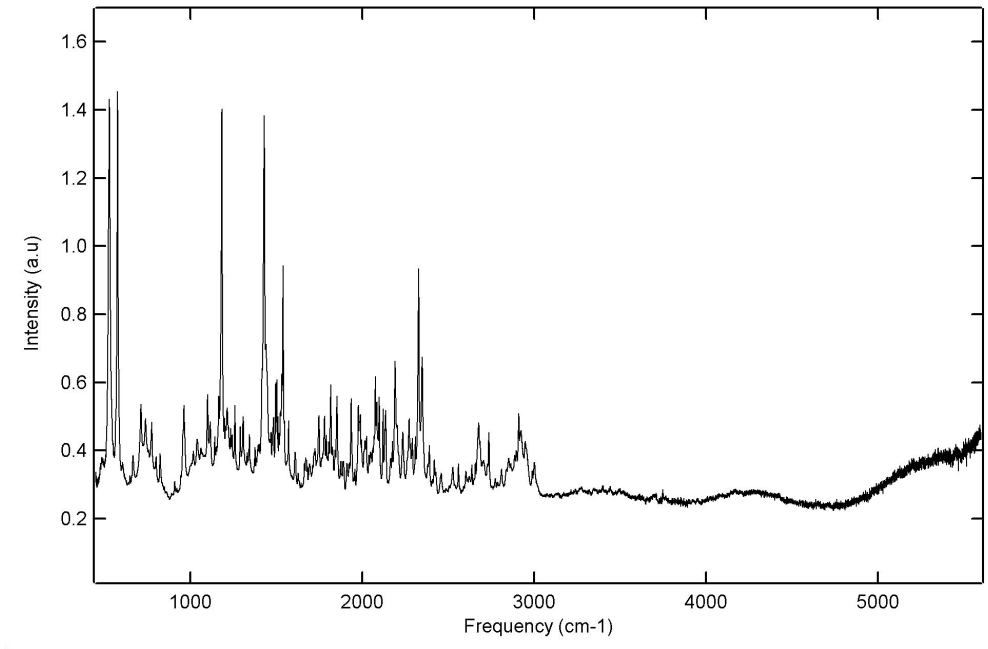

Figure 5.3: Absorption of pure C_{60}

powder. From Figure 5.3 we can see that the C_{60} has almost no absorbance in the region of the H_2 fundamental data (3500 to 5500 cm^{-1}), while the pure rotational data at about 800 cm^{-1} are in the midst of a forest of C_{60} absorbance peaks.

In attempt to see the rest of the pure rotational peaks, we switched to a broadband MCT detec-

tor. With this detector we produced the absorbance spectrum shown in Figure 5.4[3] which was taken

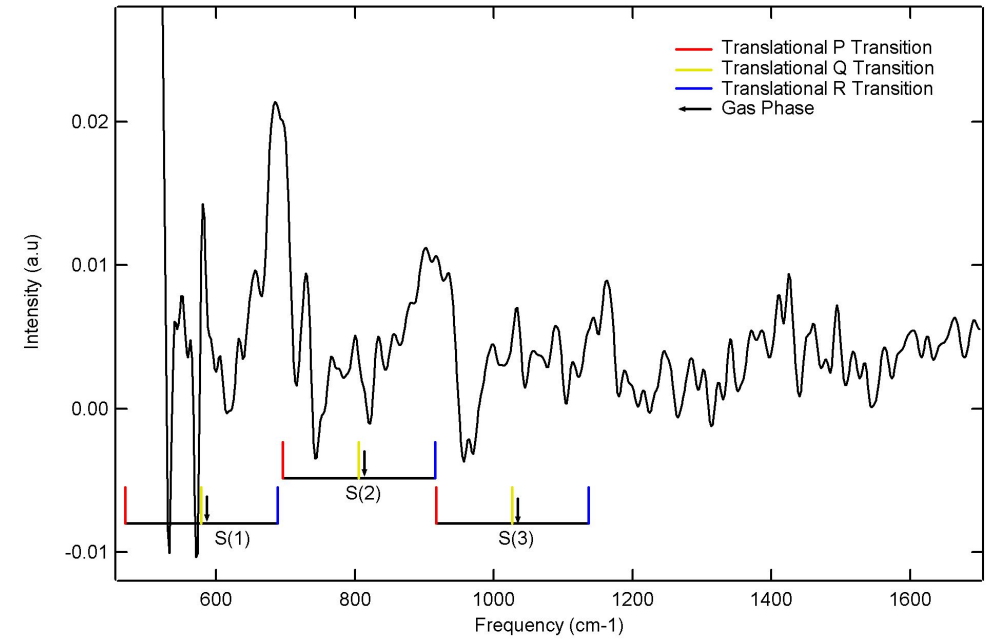

Figure 5.4: Pure rotational data of H_2 taken with the broadband MCT detector

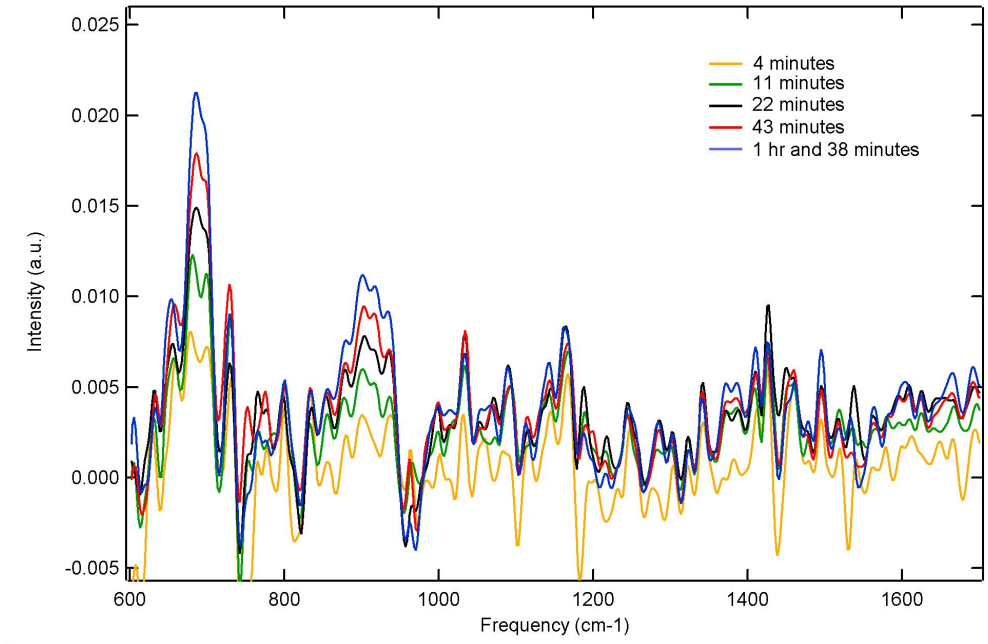

Figure 5.5: Progression spectra of the pure rotational data taken with the broadband MCT detector

[3]The data for this Figure was taken on January 18, 2005. It is an average of files 29, 30, and 32 referenced to 17 and binomial smoothed 10 points.

under otherwise identical conditions to the spectrum taken with the high sensitivity MCT detector. The broadband detector is able to detect frequencies down to about 600 cm^{-1}, but it has about two orders of magnitude less sensitivity than the other MCT detector. In this spectra we are able to detect the $S_R(1)$ peak which we couldn't see before, but now the $S_R(3)$ peak is basically lost in the noise. In the pure rotational data there is a much smaller shift from the gas phase transitions (about 8 cm^{-1}), and the translational sidebands now appear to be located at ± 110 cm^{-1} instead of the ± 127 cm^{-1} seen in the fundamental data. With the broadband detector we were able to see the peaks grow as the hydrogen diffused into the C_{60} lattice overtime (Figure 5.5[4]). This gives us confidence that they are in fact due to the hydrogen absorption and not just artifacts due to some other source.

Lastly, we used the high sensitivity MCT detector to record a spectrum of the vibrational fundamental of deuterium. The absorption spectrum for D_2 shown in Figure 5.6[5] was taken with the

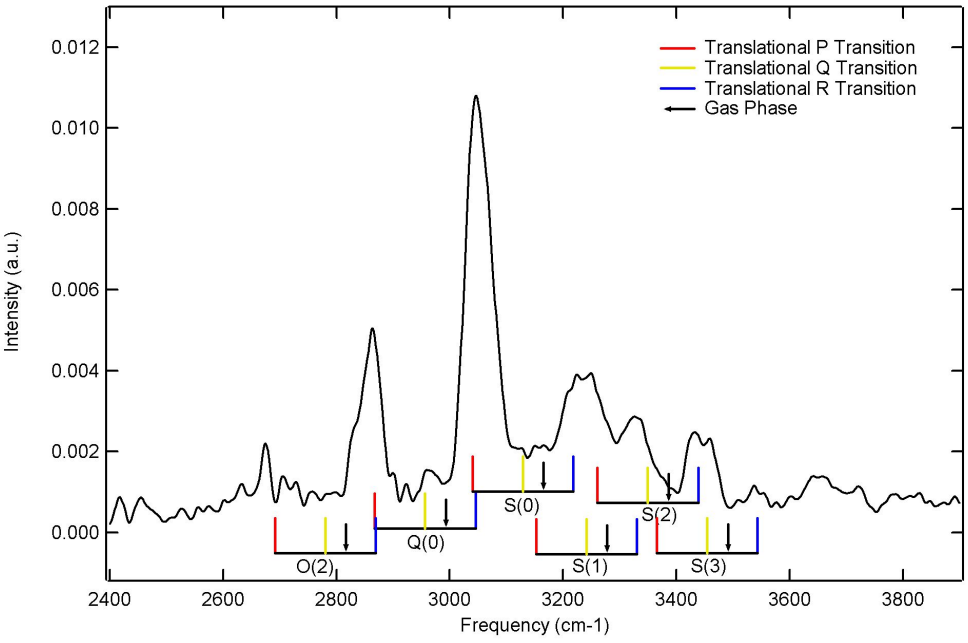

Figure 5.6: Vibrational fundamental data of D_2 taken with the high sensitivity MCT detector

same C_{60} powder and at the same loading pressure (1460 psi) as the H_2 data. This spectrum was created by averaging 4000 scans taken from 40 minutes to an hour and a half after loading the D_2

[4]Also taken on January 18, 2005, this Figure shows files 19, 22, 23, 25, and 30 all referenced to 17.

[5]The data for this Figure was taken on November 19, 2004. It is an average of files 29-33, 35, 36, and 40 referenced to 16.

gas. After this time we did not get any good spectra because the spectrometer was having trouble maintaining alignment. Like the H_2 data, the averaged raw spectrum for the D_2 data was referenced to a spectrum taken 4 minutes after the gas was introduced to the system in order to reduce the broad, collision-induced absorption feature. The noise in this spectrum is much worse than for the H_2 fundamental data making it more difficult to deconvolute the various transition peaks. The increased noise could be due to the fact that this data is at the edge of the C_{60} absorption 'forest', or it could simply be due to the problems we had maintaining alignment. The intensity of the absorbance peaks is also down by about a factor of three from the H_2 data which makes the noise appear much worse. The peak assignments given in Figure 5.6 were derived from the parameters of the fit to the H_2 data. The translational sidebands were set at $\pm\frac{127}{\sqrt{2}} = \pm 89$ cm^{-1} and a constant red-shift from the gas phase was set to $\frac{54}{\sqrt{2}} = 33$ cm^{-1}.

Chapter 6

Analysis and Interpretation

6.1 Deconvolution of the Peaks

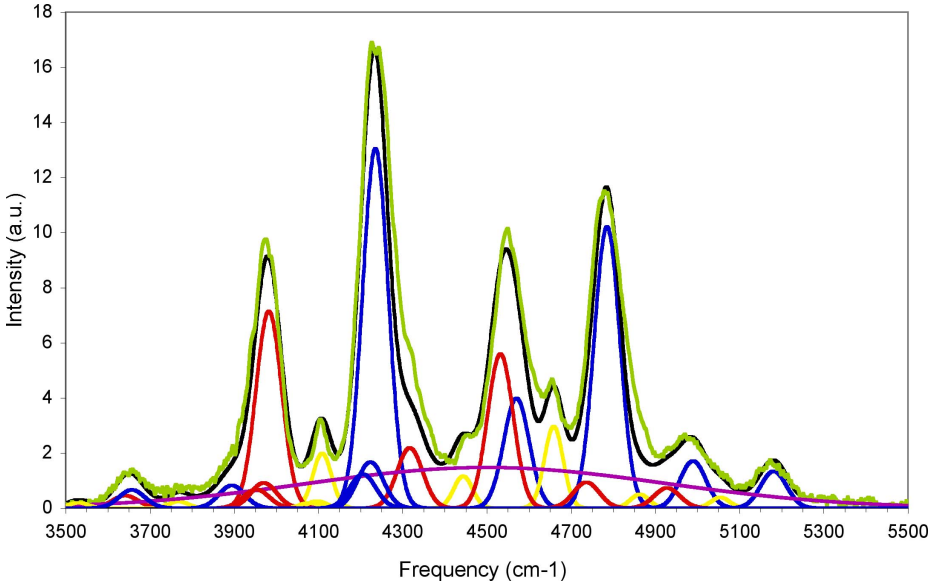

Figure 6.1: Deconvolution of the peaks in the H_2 vibrational fundamental

The above Figure represents our best interpretation and deconvolution of the absorption peaks seen in the data of the vibrational fundamental of hydrogen in C_{60}. The green curve shows the raw data given in Figure 5.1. The red, yellow, blue and purple curves are gaussians used to create our fit (the black curve) which is simply the sum of the gaussians. The red, yellow and blue gaussians represent the translational P, Q and R peaks ($\Delta n = -1, 0$, and $+1$) for each of the vibrational ($Q(0), Q(1), Q(2)$, and $Q(3)$) and rotational-vibrational ($S(0), S(1), S(2), S(3), O(2)$, and $O(3)$) branches. The fit created in this Figure was made with 15 free parameters: the width of the

center Q gaussians (1); the width of the P and R gaussians (1); the intensity ratio of the center Q gaussians to the R gaussians for the rotational-vibrational transitions (the S and O branches) and for the vibrational transitions (the Q branches) (2); the width and height of the broad (purple) gaussian (2); the transition frequency shifts from gas phase hydrogen (2); and the intensities for the R gaussians of each branch (7). (Since the Q branches are all located at basically the same frequency their intensities are adjusted as a single free parameter.) For Figure 6.1, the intensities of the R gaussains for each branch are freely adjusted to fit the data, but in the intensity analysis part of this chapter, these values are set by theoretical calculations thus cutting our number of free parameters in half. The ratio of the center Q peaks to the R peaks for all of the rotational-vibrational branches was held at 21% for and for the vibrational (Q) branch it was set at 11%. The intensity ratio of the P to the R gaussians was not a free parameter. It was theoretically calculated based on the thermal population of the translational n levels and is held constant for all branches. Thermal population is explained in detail in a later section.

The widths of the center Q gaussians and of the P and R gaussians were adjusted to fit the data and are held fixed for all branches at 51.8 and 71.5 cm^{-1} respectively. While we haven't been able to predict the numerical values for these widths, we do have a qualitative understanding of where the widths are coming from. For most purposes we assume that the potential in an octahedral site is that of a spherical simple harmonic oscillator, but this is only an approximate model and not completely accurate. Chapter 2 mentions that there is a change in the potential with orientation of about 1.8% and that even for displacements up to 0.5 Å, the potential is only *approximately* that of a simple harmonic oscillator. Even though slight, these deviations will introduce anharmonicity meaning that the translational energy levels won't have exactly equal spacing. A single peak in our spectrum such as $S_R(1)$ is made up of many different translational transitions with energies,

$$\begin{aligned} E_{S_R(1)} &= E_{vib(\nu=1)} + E_{rot(J=3)} + E_{trans(n_f=i+1)} \\ &\quad -[E_{vib(\nu=0)} + E_{rot(J=1)} + E_{trans(n_i=i)}], \end{aligned} \tag{6.1}$$

where i could be any thermally populated n level. Anharmonicity causes these energies to vary ever so slightly such that a $S_R(1)$ transition with $n_i = 0$ and $n_f = 1$ will occur at a slightly different frequency than a $S_R(1)$ transition with $n_i = 1$ and $n_f = 2$. These different transitions are at close enough frequencies that they are not resolved in our spectrum and instead just result in a single, wider peak.

The broad, purple gaussian was introduced to improve our fit to the data. It was made to replicate the collision-induced absorption spectrum of high pressure hydrogen given in [11]. As mentioned in Chapter 5, however, the absorption spectrum given in this Figure was created by referencing the raw spectrum to another spectrum taken immediately after the hydrogen gas was added to the system, thus the collision-induced absorption of the gas should have cancelled out. Another possible explanation for why the broad gaussian is needed is that it corresponds to H_2 molecules that were hopping between octahedral sites at the time of measurement which introduce a broad absorbance feature. Statistically there should be very few of these molecules that are in the process of hopping at any given instant, but they will be in a tight region between the C_{60} molecules where the potential is much greater. The greater potential will cause the induced dipole moment of these transitioning molecules to be much greater than those located in the octahedral sites and therefore they would have much more absorption. The absorption of these hopping molecules will occur over a broad range of frequencies instead of the discrete frequencies of the molecules in the octahedral sites because they will not rotate freely. Thus their rotational energies will consist of a strong mixing of the energy levels of a free quantum rotator. The result would be a broad absorbance feature such as that modeled by the purple gaussian.

6.2 Peak Placement

As mentioned in the Procedure Section and the Experimental Results Chapter, by pumping out the vacuum of the MCT detector before cooling it with LN_2, we greatly reduced the water absorption lines which had previously made it impossible to identify the O branches located at the same frequencies. Unable to see the O branches, it was believed that the S, Q, and O branches all had a constant red-shift from the gas phase of 54 cm^{-1} when intercalated in C_{60} due to interaction with the C_{60} potential [4]. Such a shift that is constant for all transitions would have to be due to a shift in the vibrational energy levels because we are looking at the vibrational fundamental and the only thing that is constant for all the transitions is that they start in the $\nu = 0$ level and end in the $\nu = 1$ level. Once we were able to see the O branches and compared the data with our fit using a constant 54 cm^{-1} shift, it was clear that this shift did not accurately place the O branches. Figure 6.2 shows this fit in red, which clearly doesn't line up with the peak in the data shown in green. It was not possible to produce a fit that lined up with the S, Q and O branches using a constant shift of the transition frequencies from the gas phase. In order to create a shift which varies for the S, Q and

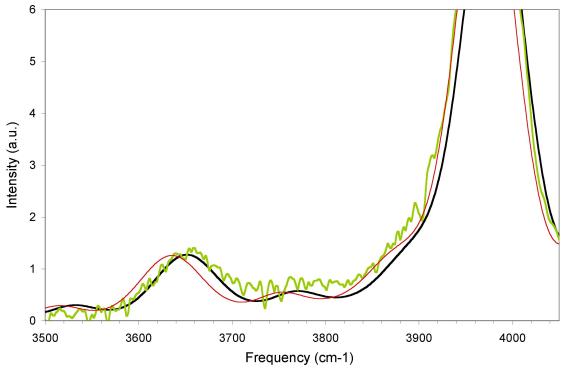

Figure 6.2: Shift of the O branches

O branches, on top of the constant vibrational shift, we introduced a shift in the rotational J levels implying that the H_2 molecules are not rotating perfectly freely in the octahedral sites. While we needed the shift to vary between the different types of branches, in order to fit to the data we also needed it to be constant for the same types of branches; the shift for $S(0)$, $S(1)$, $S(2)$ and $S(3)$ must be constant. By perturbing the J levels by an amount proportional to J, ΔJ, we were able to fill this requirement. From Figure 6.3 we can see, for example, that the transition energy for an S branch of

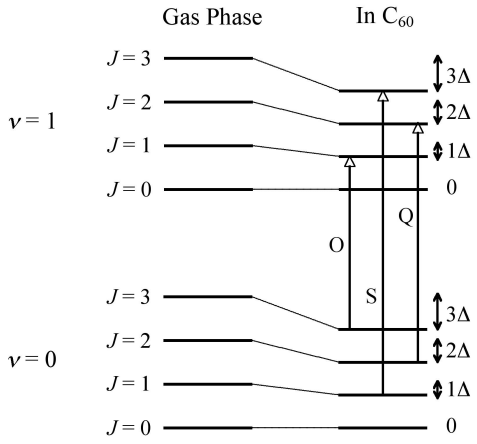

Figure 6.3: Shifts of the rotational J levels

H_2 in C_{60} versus in the gas phase will be:

$$E_{in\ C_{60}} = [E(J+2) - \Delta(J+2)] - [E(J) - \Delta J] \quad (6.2)$$

$$= E(J+2) - E(J) - \Delta J + \Delta J - 2\Delta \quad (6.3)$$

$$= E(J+2) - E(J) - 2\Delta \quad (6.4)$$

$$= E_{gas\ phase} - 2\Delta. \quad (6.5)$$

Thus the shift does not depend on J, and will be the same for all S branches. Similar derivations for the O and Q branches shows that the rotational shift for these branches will be -2Δ and 0 respectively. Thus in combination with the constant vibrational red-shift, ν_{shift}, we have,

$$E_{in\ C_{60}} = \begin{cases} E_{gas\ phase} - \nu_{shift} - 2\Delta & \text{for } S \text{ branches} \\ E_{gas\ phase} - \nu_{shift} & \text{for } Q \text{ branches} \\ E_{gas\ phase} - \nu_{shift} + 2\Delta & \text{for } O \text{ branches} \end{cases} \tag{6.6}$$

The best fit was achieved with $\Delta = 4$ cm^{-1} and $\nu_{shift} = 46$ cm^{-1} giving shifts from the gas phase of 54, 46, and 38 cm^{-1} for the S, Q and O branches respectively. These values were used to create the fit in Figure 6.1 at the beginning of this chapter and the black curve in Figure 6.2.

The shift from the gas phase for the pure rotational transitions will not have ν_{shift} because $\Delta\nu = 0$ so a perturbation in the vibrational energy levels will not have an effect on the energy of the transitions. If the above parameters are the same for the pure rotational transitions then, we should expect to see a red-shift from the gas phase frequency of $2\Delta = 8$ cm^{-1} in the S branches. Unfortunately, due to the level of noise in the pure rotational data we are unable to identify the center Q peaks. Judging only from the location of the R peaks, a shift of 8 cm^{-1} would fit the data if the translational sidebands are located at ± 110 instead of ± 127 cm^{-1}. We are still investigating why there might be this change in the location of the sidebands from the vibrational fundamental.

6.3 Intensity

In the deconvolution fit for the vibrational fundamental given at the beginning of this chapter, the relative intensities of the different branches were all free parameters, which explains why we were able to produce such a good fit to the data. In order to see how our experimental results compare with theoretical predictions, we calculated the intensities of each branch as explained step-by-step below, and then used these values to create a new fit to the data with only seven remaining free parameters, a reasonable number considering we are fitting a total of at least 21 peaks.

As mentioned in the discussion of selection rules given in Chapter 3, the absorption of the hydrogen molecules actually mimics Raman spectroscopy rather than IR spectroscopy. Condon explains that the IR absorption of a normally IR-inactive molecule like H_2 when placed in an electric field is completely analogous to the Raman effect [24]. In Raman, the induced dipole moment of

the molecule is due to the electric vector of the incident light wave while in our case it is due to the electric field of the surrounding C_{60} molecules. Therefore, when calculating the intensities for our peaks, we use the accepted equations for Raman rather than IR absorption. According to Hertzberg [18], the intensity of an absorption line in Raman spectroscopy corresponding to a transition from state ψ_a to state ψ_b is determined by

$$I = \nu \left(I_0 \frac{8\pi^3 N}{3hcQ_r} \right) \sum_{m,m'} |\langle \psi_a \mid \mu_{ind} \mid \psi_b \rangle|^2 e^{\frac{-B_\nu J(J+1)}{T}}, \tag{6.7}$$

where ν is the frequency of the transition; I_0 is the intensity of the incident radiation; N is the number of molecules; Q_r is the partition function; $e^{\frac{-B_\nu J(J+1)}{T}}$ is the thermal population of the J^{th} rotational energy level; and $\langle \psi_a \mid \mu_{ind} \mid \psi_b \rangle$ is the matrix element of the induced dipole moment between an initial state with quantum numbers ν, n, J and m, and a final state with quantum numbers ν', n', J' and m'. A factor of 1.44 is included for unit conversion when B_ν, the rotational constant, is expressed in cm^{-1} in order to get the numerator and denominator in the same units of energy. For our purposes, we are only interested in the relative intensities, so the term in parentheses in Equation (6.7) which is constant for all the branches will be ignored. The next sections explain how the various elements of this equation were calculated for our fit.

6.3.1 Thermal Population

The intensity of an absorption peak for a given transition depends on the number of molecules that undergo thE particular transition because the more molecules absorbing radiation at a specific frequency, the more the incident radiation will be lowered at that frequency relative to our background spectrum, and thus the larger the peak when the two spectra are referenced. The number of molecules that undergo a transition is directly related to the population of the transition's initial state. The Maxwell-Boltzmann distribution law tells us that the population of a particular energy level with energy E is proportional to the Boltzmann factor,

$$e^{-E/kT}, \tag{6.8}$$

where k is the Boltzmann constant and T is the absolute temperature [18]. Thus, the relative thermal population for different rotational J levels is given by substituting the corresponding rotational energies for E. As is evident from Equation (6.7), for this calculation of the relative branch intensities we used the rotational energies of a rigid rotator instead of the true energies which represent a

mixing of these levels coming from the vibrational perturbation. The difference is slight and within our experimental determination of the intensities.

From Equation (6.8) we see that at constant temperature, there is an exponential decay in level population with increasing energy. Since the translational P peaks correspond to $\Delta n = -1$, the ground state P transition originates in the $n = 1$ state unlike the R, $\Delta n = +1$, peaks which have their ground state transition originating in the $n = 0$ level. This implies that the P peaks in our spectrum should be less intense than the R peaks because they have less thermal population in their initial states. The ratio of the P to R branch intensities will be equal to

$$e^{-\Delta E/kT},$$

where ΔE is the energy difference between the n and the $n+1$ translational energy levels. Treating the translational motion as that of a spherical simple harmonic oscillator, Equation (3.12) shows that the energy level spacing is constant and equal to n_o. Using the experimentally determined value of $n_o = 127$ cm^{-1}, the P to R ratio at room temperature is 0.55. This value for the ratio of the P to R intensities is used in all fits to the data and held constant for every branch.

6.3.2 Dipole Moment Matrix Elements

As introduced in Chapter 3, the induced dipole moment of an H_2 molecule in an octahedral site can be calculated from

$$\vec{\mu}_{ind} = \alpha \vec{E}_{C_{60}}, \tag{6.9}$$

where α is the polarizability tensor and $E_{C_{60}}$ is the electric field due to the C_{60} molecules at the location of the H_2 molecule. When expressed in terms of a coordinate system chosen such that the Z' axis is parallel to the molecular axis of the hydrogen molecule, the polarizability tensor is

$$\alpha_{X'Y'Z'} = \begin{pmatrix} \alpha_\perp & 0 & 0 \\ 0 & \alpha_\perp & 0 \\ 0 & 0 & \alpha_\parallel \end{pmatrix}. \tag{6.10}$$

Modeling the potential of an octahedral site as a spherical simple harmonic oscillator, we find that

$$\vec{E}_{C_{60}} = -A\vec{R}, \tag{6.11}$$

where $\vec{R}$ is the displacement vector of the center of mass of the H_2 molecule from the center of the site and A is a constant. Next we choose a fixed coordinate system such that the incoming photon

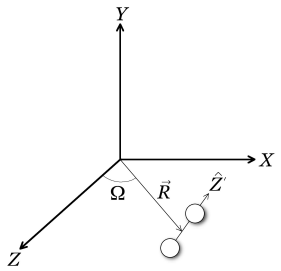

Figure 6.4: Identification of Ω and $\vec{R}$

is polarized in the Z direction (meaning its electric field vector points in the Z direction) and the center of mass of the H_2 molecule lies in the X-Z plane (see Figure 6.4). Thus $\vec{R}$ has no component in the Y direction:

$$\vec{R}_{XYZ} = \begin{pmatrix} R_X \\ 0 \\ R_Z \end{pmatrix}. \tag{6.12}$$

If we define Ω as the angle between $\vec{R}$ and the Z axis then we can rewrite (6.12) as

$$\vec{R}_{XYZ} = \begin{pmatrix} R\sin\Omega \\ 0 \\ R\cos\Omega \end{pmatrix}. \tag{6.13}$$

We later return to this form of $\vec{R}$.

In order to calculate the induced dipole moment we must find the product of the polarizability tensor and $\vec{E}_{C_{60}}$, however, they are currently defined relative to different coordinate systems; the molecular $X'Y'Z'$ basis and the fixed XYZ basis. Before we can multiply the two together, we must

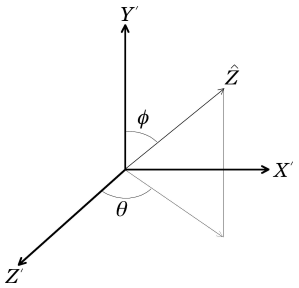

Figure 6.5: Identification of θ and ϕ

rotate $\vec{R}$ so that we can express $\vec{E}_{C_{60}}$ in terms of the molecular coordinate system. Using the polar

angles θ and ϕ to describe the molecular coordinate system relative to the fixed system (see Figure 6.5), we can then use rotation matrices to determine

$$\vec{R}_{X'Y'Z'} = \begin{pmatrix} \cos\theta & 0 & -\sin\theta \\ 0 & 1 & 0 \\ \sin\theta & 0 & \cos\theta \end{pmatrix} \begin{pmatrix} \cos\phi & \sin\phi & 0 \\ -\sin\phi & \cos\phi & 0 \\ 0 & 0 & 1 \end{pmatrix} \begin{pmatrix} R_X \\ 0 \\ R_Z \end{pmatrix} = \begin{pmatrix} R_X\cos\theta\cos\phi - R_Z\sin\theta \\ -R_X\sin\phi \\ R_Z\cos\theta + R_X\cos\phi\sin\theta \end{pmatrix}. \tag{6.14}$$

It is now possible to find $\mu_{ind,X'Y'Z'}$, but unfortunately we actually need $\mu_{ind,XYZ}$, because we chose the polarization of the incoming photon relative to the fixed coordinate system, and it is the electric field vector of the photon that will interact with the induced dipole moment to cause a transition in the molecule. Thus after finding $\alpha_{X'Y'Z'}\vec{R}_{X'Y'Z'}$, we use the inverse rotation matrices to rotate the result back to the X, Y, Z system:

$$\mu_{ind,XYZ} = -A \begin{pmatrix} \cos\phi & -\sin\phi & 0 \\ \sin\phi & \cos\phi & 0 \\ 0 & 0 & 1 \end{pmatrix} \begin{pmatrix} \cos\theta & 0 & \sin\theta \\ 0 & 1 & 0 \\ -\sin\theta & 0 & \cos\theta \end{pmatrix} \begin{pmatrix} \alpha_\perp & 0 & 0 \\ 0 & \alpha_\perp & 0 \\ 0 & 0 & \alpha_\parallel \end{pmatrix} \begin{pmatrix} R_X\cos\theta\cos\phi - R_Z\sin\theta \\ -R_X\sin\phi \\ R_Z\cos\theta + R_X\cos\phi\sin\theta \end{pmatrix}. \tag{6.15}$$

We only care about the Z component of the induced dipole moment, $\mu_{ind,Z}$, because the photon is polarized in the Z direction. The expression above gives

$$\mu_{ind,Z} = -A\left(R_X(\alpha_\parallel - \alpha_\perp)\cos\theta\sin\theta\cos\phi + R_Z(\alpha_\perp\sin^2\theta + \alpha_\parallel\cos^2\theta)\right). \tag{6.16}$$

Substituting for the components of $\vec{R}$ in terms of Ω (see Equations (6.12) and (6.13)), we find

$$\mu_{ind,Z} = -A\left(R\sin\Omega(\alpha_\parallel - \alpha_\perp)\cos\theta\sin\theta\cos\phi + R\cos\Omega(\alpha_\perp\sin^2\theta + \alpha_\parallel\cos^2\theta)\right). \tag{6.17}$$

The polarizability of a molecule is more often described in terms of an anisotropic term, $\Delta\alpha$, and an isotropic term, $\bar{\alpha}$ which can be calculated from $\alpha_\parallel$ and $\alpha_\perp$ with the following expressions,

$$\Delta\alpha = \alpha_\parallel - \alpha_\perp \tag{6.18}$$

and

$$\bar{\alpha} = \frac{1}{3}(\alpha_\parallel + 2\alpha_\perp). \tag{6.19}$$

Using these expressions, Equation (6.17) can be rewritten as

$$\mu_{ind,Z} = -AR\left[-\sqrt{\frac{2\pi}{15}}\left(Y_2^1 - Y_2^{-1}\right)\Delta\alpha\sin\Omega + \frac{4}{3}\sqrt{\frac{\pi}{5}}Y_2^0\Delta\alpha\cos\Omega + \sqrt{4\pi}Y_0^0\bar{\alpha}\cos\Omega\right], \tag{6.20}$$

where Y_J^m represent the spherical harmonics.

From Equation (6.7), in order to calculate the relative intensities of the various molecular transitions we need to find

$$|\langle \psi_a \mid \mu_{ind,Z} \mid \psi_b \rangle|^2, \tag{6.21}$$

where ψ_a and ψ_b are the initial and final states of the transition. Using the equation for the induced dipole moment given in (6.20), the matrix element can be broken up as,

$$\begin{aligned} &\langle \psi_a \mid \mu_{ind,Z} \mid \psi_b \rangle = \\ &-A\langle n \mid R \mid n' \rangle \langle Jm \mid -\sqrt{\frac{2\pi}{15}} \left(Y_2^1 - Y_2^{-1} \right) \Delta\alpha \sin\Omega + \frac{4}{3}\sqrt{\frac{\pi}{5}} Y_2^0 \Delta\alpha \cos\Omega + \sqrt{4\pi} Y_0^0 \bar{\alpha} \cos\Omega \mid J'm' \rangle. \end{aligned} \tag{6.22}$$

(As a side note, this expression reconfirms the selection rule for ΔJ given in Chapter 3, because it is immediately clear from the spherical harmonics that for this expression to be nonzero it must be the case that $\Delta J = 0, \pm 2$.) Remembering that what we are interested in is the relative intensities of the $Q(0)$, $Q(1)$, $Q(2)$, $Q(3)$, $S(0)$, $S(1)$, $S(2)$, $S(3)$, $O(2)$ and $O(3)$ branches, we can ignore the $-A\langle n \mid R \mid n' \rangle$ in Equation (6.22) because we need only to consider the terms which will vary with different combinations of J and J'. Everything else will cancel out when we ratio the intensities. In addition, when these matrix elements are substituted into Equation (6.7) they will be summed over all values of m and m'. This allows us to also ignore the $\sin\Omega$ and $\cos\Omega$ because when summed over all m and m', these factors will contribute equally to each term and thus will divide out in the relative intensities. Thus we have for the different branches:

$$S(J) : \sum_{m,m'} \left[-\sqrt{\frac{2\pi}{15}} \left(\langle Y_J^m \mid Y_2^1 \mid Y_{J+2}^{m'} \rangle - \langle Y_J^m \mid Y_2^{-1} \mid Y_{J+2}^{m'} \rangle \right) \Delta\alpha + \frac{4}{3}\sqrt{\frac{\pi}{5}} \langle Y_J^m \mid Y_2^0 \mid Y_{J+2}^{m'} \rangle \Delta\alpha \right]^2 \tag{6.23}$$

$$O(J) : \sum_{m,m'} \left[-\sqrt{\frac{2\pi}{15}} \left(\langle Y_J^m \mid Y_2^1 \mid Y_{J-2}^{m'} \rangle - \langle Y_J^m \mid Y_2^{-1} \mid Y_{J-2}^{m'} \rangle \right) \Delta\alpha + \frac{4}{3}\sqrt{\frac{\pi}{5}} \langle Y_J^m \mid Y_2^0 \mid Y_{J-2}^{m'} \rangle \Delta\alpha \right]^2 \tag{6.24}$$

$$\begin{aligned} Q(J) : \sum_{m,m'} \Bigg[&-\sqrt{\frac{2\pi}{15}} \left(\langle Y_J^m \mid Y_2^1 \mid Y_J^{m'} \rangle - \langle Y_J^m \mid Y_2^{-1} \mid Y_J^{m'} \rangle \right) \Delta\alpha + \frac{4}{3}\sqrt{\frac{\pi}{5}} \langle Y_J^m \mid Y_2^0 \mid Y_J^{m'} \rangle \Delta\alpha \\ &+ \sqrt{4\pi} \langle Y_J^m \mid Y_0^0 \mid Y_J^{m'} \rangle \bar{\alpha} \Bigg]^2 . \end{aligned} \tag{6.25}$$

The last term in Equation (6.25) involving the isotropic polarizability, $\bar{\alpha}$, and the Y_0^0 spherical harmonic is called the trace-scattering term [18]. This term only contributes to the intensity of the

Q branches and not to the S and O branches. The reason for this can be understood using a classical picture of the hydrogen molecule undergoing a rotational transition. Recall that a Q branch has $\Delta J = 0$ while the S and O branches have $\Delta J = +2$ and $\Delta J = -2$. Classically, an increase (decrease) in J corresponds to an increase (decrease) in the angular momentum of the hydrogen molecule. In order for the incoming photon to cause such a change in the angular momentum it would have to exert a torque on the molecule. A torque can only be produced by interacting with the anisotropic polarizability, $\Delta\alpha$, because the isotropic polarizability, $\bar{\alpha}$, has no directionality associated with it.

We used Mathematica to evaluate the sums in equations (6.23), (6.24), and (6.25) for all possible values of m and m'. The solutions turn out to agree exactly with those arrived by James and Klemperer for the line intensities of diatomic molecules in the Raman effect [25]:

$$S(J) : \frac{7}{30}|\langle \nu J \mid \Delta\alpha \mid \nu' J' \rangle|^2 K(J+1) \tag{6.26}$$

$$O(J) : \frac{7}{30}|\langle \nu J \mid \Delta\alpha \mid \nu' J' \rangle|^2 K(J-1) \tag{6.27}$$

$$\begin{aligned} Q(J) : (2J+1)|\langle \nu J \mid \bar{\alpha} \mid \nu' J' \rangle|^2 + \frac{1}{15}|\langle \nu J \mid \Delta\alpha \mid \nu' J' \rangle|^2 \frac{J(J+1)(2J+1)}{(2J+3)(2J-1)} \\ + |\langle \nu J \mid \Delta\alpha \mid \nu' J' \rangle|^2 \left(-\frac{2J+1}{9} + \frac{4}{15} K(J) \right) \end{aligned} \tag{6.28}$$

where

$$K(J) = \frac{J(J+1)}{(2J+1)} \text{ and } H(J) = \frac{J(4J^2+1)}{(2J+1)(2J-1)}. \tag{6.29}$$

With the values calculated by Schwartz and LeRoy [26] for the polarizability matrix elements of H_2, we determined the sums of the matrix elements, $\sum_{m,m'}|\langle \psi_a \mid \mu_{ind,Z} \mid \psi_b \rangle|^2$, for each branch in our spectrum of the vibrational fundamental.

6.3.3 Orthohydrogen and Parahydrogen

Now that we have calculated the matrix elements we have everything we need to use Equation (6.7), however, there is another factor that needs to be incorporated to find the relative intensities of the different branches which is not taken into account in that equation: the relative concentrations of orthohydrogen and parahydrogen.

Hydrogen molecules are made up of two protons which are indistinguishable fermions and so the Spin-Statistics Theorem requires that the total molecular wavefunction be anti-symmetric. The total wavefunction is a product of a spatial part, the spherical harmonics, and a spin part, a singlet or a

triplet state. If $\hat{P}$ is the parity operator, is can be shown that

$$\hat{P}(Y_J^m(\theta,\phi)) = Y_J^m(\pi-\theta,\pi+\phi) = (-1)^J Y_J^m(\theta,\phi). \tag{6.30}$$

From this it is clear that for even values of J, the spatial part of the wavefunction will be symmetric so the spin part must be anti-symmetric, while if J is odd the spatial part will be anti-symmetric and the spin part must be symmetric. Since protons are spin $\frac{1}{2}$ particles, the total spin part of the molecular wavefunction is either $s=0$ (the anti-symmetric singlet state) or $s=1$ (the symmetric triplet state) which correspond to the following possible combinations of spin states for the two protons:

$$\left\{ \begin{array}{l} |\uparrow\uparrow\rangle \\ \frac{1}{\sqrt{2}}\left(|\uparrow\downarrow\rangle + |\downarrow\uparrow\rangle\right) \\ |\downarrow\downarrow\rangle \end{array} \right\} s=1 \text{ (triplet)} \tag{6.31}$$

$$\left\{ \begin{array}{l} \frac{1}{\sqrt{2}}\left(|\uparrow\downarrow\rangle - |\downarrow\uparrow\rangle\right) \end{array} \right\} s=0 \text{ (singlet)}. \tag{6.32}$$

Hydrogen with $s=1$ is called orthohydrogen and hydrogen with $s=0$ is called parahydrogen. Because the $s=1$ triplet state is three fold degenerate, while the $s=0$ state is singly degenerate, at room temperature, there is a 3:1 ratio of ortho to parahydrogen. This ratio implies that on top of the equation for the thermal population of the different J levels, we need to include the fact that there will be three times as many molecules in the odd J levels than are in the even J levels due to the relative concentrations of ortho and parahydrogen. To take this into account, we multiplied Equation (6.7) by 3 for transitions beginning in states with odd J values and by 1 for transitions beginning in states even J values.

6.3.4 Intensities of the Q Branches

We calculated the relative intensities for each branch in our spectrum using

$$\begin{array}{ll} I \propto (3)\nu \sum_{m,m'} |\langle \psi_a \mid \mu_{ind} \mid \psi_b \rangle|^2 e^{\frac{-B_\nu J(J+1)}{T}} & \text{for } J \text{ odd} \\ I \propto (1)\nu \sum_{m,m'} |\langle \psi_a \mid \mu_{ind} \mid \psi_b \rangle|^2 e^{\frac{-B_\nu J(J+1)}{T}} & \text{for } J \text{ even} \end{array} \tag{6.33}$$

where ν is the frequency of the transition and J is the rotation quantum number of the initial state. We used the values resulting from these calculations for the relative intensities of the gaussians corresponding to the translational R peaks in our deconvolution. The intensities of the P and Q peaks for

each branch are defined relative to the R peak intensities by the calculated P to R ratio and a free parameter for the intensity of the Q peaks as a percentage of the R peak intensity which was held fixed for all branches at 21%. Using these calculations, we produced the fit shown in black in Figure 6.6. It is immediately clear that this is a terrible fit to the data (shown in green). The intensities of

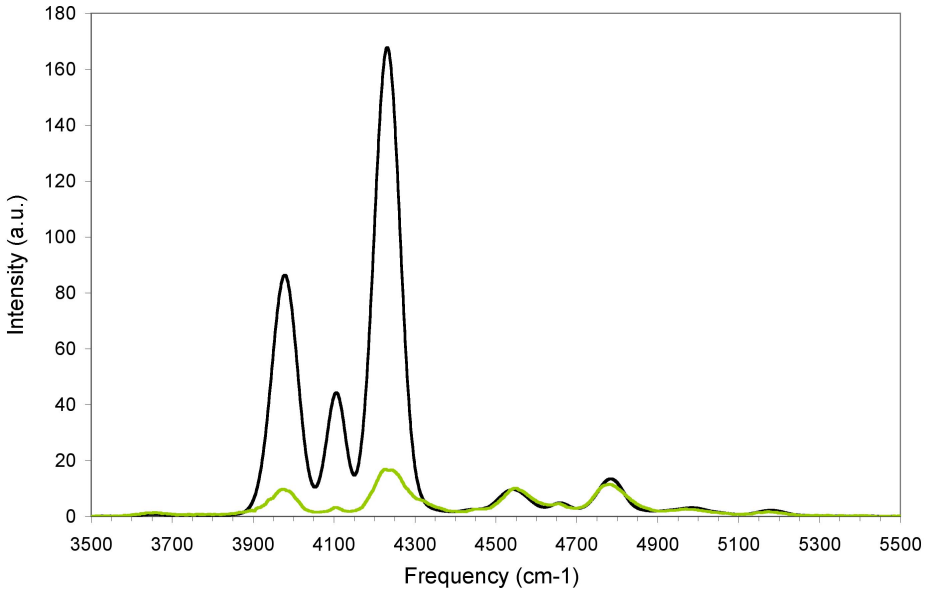

Figure 6.6: Intensities calculated with Equation (6.33)

the Q branches are way too high. Recalculating the relative intensities without the trace term for the Q branches, we produced the black fit in Figure 6.7. This fit is greatly improved, but we have no theoretical basis for not including the trace term, and the intensities of the translational sidebands of the Q branches from this calculation still don't agree well with the data. Without the Q branches over dominating the fit, we can see in Figure 6.7 that the calculated intensities for the rest of the peaks in the spectrum are not far off the experimental data.

The question now is, why are the intensities of our Q branches roughly the same as those of the S branches when the theoretical calculation predicts them to be much larger? Looking at Raman data for the absorption of pure hydrogen [27] we see that these spectra do in fact show the domination of the Q branch intensities as predicted by our theoretical calculation. This implies that there must be something special about our situation with the hydrogen intercalated in C_{60} that causes the intensities of the Q branches to no longer completely overshadow the S branches. We are still investigating the answer to this question but have developed a possible explanation.

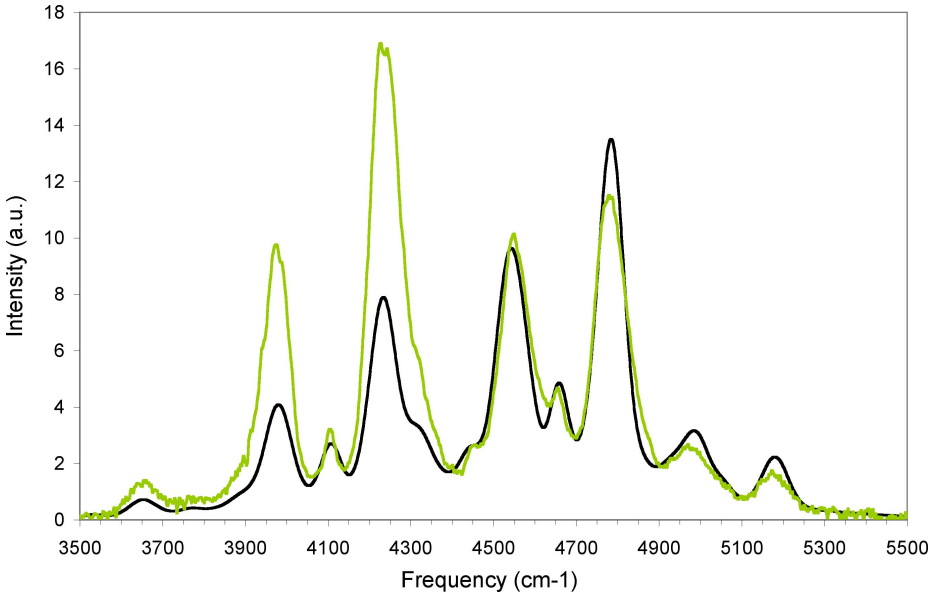

Figure 6.7: Intensities calculated with Equation (6.33) without the trace term

The incident radiation for the vibrational fundamental has a frequency of approximately 4100 cm^{-1} and a wavelength of about 2.4 μm. This wavelength is very large compared to the van der Waals radii of both an H_2 molecule and a C_{60} molecule. Thus, the incident photons won't necessarily pin-point the hydrogen molecules in the sample. We need to consider that the absorption in our spectra is due not only to the change in the dipole moment of the hydrogen molecules, but also to the change in the dipole moment of the C_{60} molecules. Since H_2 is made up of 2 electrons and 2 protons, it has a quadrupole moment. This quadrupole moment in turn induces a dipole moment in the C_{60} molecules surrounding an octahedral site. C_{60} molecules have a very high polarizability (about 83 $Å^3$ [5]), so the induced dipole moment will be large. The quadrupole moment of the hydrogen molecule goes as the Y_2^0 spherical harmonic [28]. The matrix element of this spherical harmonic will be nonzero when $\Delta J = 0, \pm 2$, so it will contribute to the intensity of the Q, S, and O branches. Assuming that it contributes equally to each branch, if the coefficient of this term is larger than the coefficient of the Y_0^0 trace term (which is what gives the Q branch the large relative intensity), then the result would be the approximately equal intensities of the S and Q branches we see in our data.

There is some supporting evidence for this hypothesis from the relative intensities of the Q and S branches in the data presented by Hunt and Welsh [23]. Instead of inducing a dipole moment in H_2 by intercalating it within a host lattice, they use a related technique of collision-induced absorption whereby mixtures of hydrogen and other molecules are put at very high pressures and the resulting

infrared absorption spectra appear very similar to our results. In one figure we can see the intensity ratio of the Q and S branches for H_2 with N_2, Ar, and He. These have polarizabilities of 1.7, 1.4, and 0.2 $Å^3$ respectively, and the corresponding Q to S branch intensity ratios are about 2.6, 2.2, and 4.6. N_2 and Ar which have relatively similar polarizabilities have relatively similar intensity ratios that are both substantially lower than that of He which has a much lower polarizability. Thus we can suppose that C_{60} with a much higher polarizability than any of these would result in an even lower Q to S branch ratio; the branches should be approximately the same height instead of the the Q branch dominating, which is what we see in the data.

Chapter 7

Conclusions and Future Directions

This paper has presented experimental results and theoretical analysis of the induced infrared absorption of H_2 molecules within an octahedral site of a C_{60} lattice. The frequencies of the absorption peaks in vibrational fundamental of H_2 were found to have a constant red-shift from the gas phase of 46 cm^{-1} due to a perturbation in the vibrational energy levels, and the S, Q, and O branches have additional shifts of -8, 0, and +8 cm^{-1} due to a small perturbation in the rotational energy levels. Each branch has symmetrically placed translational side bands at ± 127 cm^{-1} corresponding to the quantized translational motion of the hydrogen molecules in the spherical simple harmonic oscillator potential of an octahedral site. Data of the H_2 pure rotational $S(1)$, $S(2)$, and $S(3)$ transitions shows a shift from the gas phase of about 8 cm^{-1} and translational sidebands located at ± 110 cm^{-1}. An analysis of the interaction of the incident radiation with the hydrogen molecules in an octahedral site concludes that the electric field of the C_{60} molecules causes the H_2 absorbance characteristics to resemble those of the Raman effect rather than standard IR spectroscopy. A detailed calculation of the relative intensities of the absorption peaks using equations associated with the Raman effect is found to produce values for the relative intensity of the Q branches which are an order of magnitude above those seen in the data. A possible explanation for this effect is that it is a result of the quadrupole moment of the H_2 molecules in turn inducing a dipole moment in the surrounding C_{60} molecules.

Much of the rest of my honors work this year consisted of putting the finishing touches on a box which combines a constant flow liquid helium cryostat, a DRIFTS rig, and a high pressure line. The box was designed by Professor Stephen FitzGerald and Phil Korngut and created by Bill Martin. It has CaF_2 windows and will allow us to perform the same IR measurements of H_2 within C_{60} only

with the sample at temperatures as low as 4.2 K. The sample is held under the DRIFTS rig by a copper finger attached to the base of the cryostat. In order for this finger and the sample to reach liquid helium temperature, the box must maintain a very good vacuum. After about a month of adjustments, we were able to improve the box from not holding any detectable vacuum to its current state of reaching pressures close to 10^{-6} torr with a diffusion pump.

When the sample reaches 4.2 K, there should be no thermal population of excited energy levels. With everything in its ground state we shouldn't see any P peaks or the $O(2)$, $O(3)$, $S(2)$, $S(3)$, $Q(2)$, and $Q(3)$ branches in our absorption spectra because these transitions originate in excited energy levels. Without any of these transitions, our absorption spectra will be much simpler making it much easier to confidently identify the remaining transition peaks which will have much less overlap. We should still see the $Q(1)$ and the $S(1)$ branches because the $J = 1$ level will be populated due to the presence of orthohydrogen. Orthohydrogen has odd values of J, and can only lower into the $J = 0$ state through the presence of a microscopically inhomogeneous magnetic field. Otherwise, the molecules remain trapped in the $J = 1$ level.

Additionally, the peaks that do remain in the spectrum at low temperature should become much sharper and more intense. Recall that the width of the peaks is a result of anharmonicity in the translational energy levels such that a transition from $n = 0$ to $n = 1$ doesn't occur at exactly the same frequency as a transition from $n = 1$ to $n = 2$. At low temperature, all of the hydrogen molecules should be initially in the $n = 0$, state so when excited by an incoming photon they will all undergo the same transition to the $n = 1$ state. Thus, while at room temperature a single peak is a combination of the hydrogen molecules absorbing incoming radiation over a small range of frequencies, at low temperature they will all absorb the same frequency of light resulting in a very sharp and intense absorption peak.

After many months of preparation and planning, the first experimental run with the box was performed only a few days ago. The experiment was successful and the preliminary results are very promising: in the spectra taken at low temperature we see signs only of the $Q_R(0, 1)$, $S_R(0)$, and $S_R(1)$ peaks and these are incredibly sharp and thus well separated compared to the room temperature data. Spectra so far have been taken with H_2 loaded in C_{60} at 4.2 K, 8 K, 10 K, 40 K, 70 K, and 100 K. We are currently working on taking background spectra of pure C_{60} at these temperatures

as a reference. There is much more experimental work that can be done and much analysis and interpretation of these exciting initial results.

Other future experiments might include attempts to get better, less noisy data of the H_2 pure rotational transitions that go to lower frequencies allowing us to see the rest of the transition peaks, and an experiment to see the overtone, $\Delta\nu = 2$, of H_2 in the near-infrared. Additional analysis also needs to be done on the location and intensities of the absorption peaks in the D_2 and H_2 pure rotational data.

Bibliography

[1] H. E. Hallam, *Vibrational Spectroscopy of Trapped Species* (John Wiley & Sons, London, 1973) 1-9.

[2] M. Hirscher (ed.), "Hydrogen storage in nanoscale carbon and metals" *Applied Physics A* (special issue) **72**, 129-264 (2001).

[3] L. Schilapbach and A. Züttel, "Hydrogen-storage materials for mobile applications" *Nature* **414**, 353-358 (2001).

[4] S. A. FitzGerald, S. Forth and M. Rinkoski, "Induced infrared absorption of molecular hydrogen in solid C_{60}" *Physical Review B* **65**, 140302 (2002).

[5] M. S. Dresselhaus, G. Dresselhaus, and P. C. Eklund, *Science of Fullerenes and Carbon Nanotubes* (Academic Press, San Diego, 1996).

[6] H. W. Kroto, J. R. Heath, S. C. O'Brien, R. F. Curl and R. E. Smalley, "C_{60}: Buckminsterfullerene" *Nature* **318**, 162-163 (1985).

[7] G. S. Hammond and V. J. Kuck, *Fullerenes: Synthesis, Properties, and Chemistry of Large Carbon Clusters* (American Chemical Society, Washington, DC, 1992).

[8] S. A. FitzGerald, T. Yildirim, L. J. Santodonato, D. A. Neumann, J. R. D. Copley, J. J. Rush, and F. Trouw, "Quantum dynamics of interstitial H_2 in solid C_{60}" *Physical Review B* **60**, 6439-6451 (1999).

[9] Marie Rinkosi, *Gas Storage in Fullerenes* (An Honors Thesis Presented to the Physics Department of Oberlin College, 2002).

[10] A. J. Pertsin and A. I. Kitaigorodsky, *The Atom-Atom Potential Method* (Springer-Verlag, Berlin, 1987) 73, 89.

[11] Scott Forth, *Induced Infrared Absorption of H_2 in C_{60}* (An Honors Thesis Presented to the Physics Department of Oberlin College, 2002).

[12] D. B. Chase and J. F. Rabolt, *Fourier Transform Raman Spectroscopy: From Concept to Experiment* (Academic Press, San Diego, 1994) 234-235.

[13] H. Hamaguchi, I. Suzuki, and A. D. Buckingham, "Determination of derivatives of the polarizability anisotropy in diatomic molecules. I. Theoretical considerations on vibration-rotation Raman intensities" *Molecular Physics* **43**, 963-973 (1981).

[14] D. J. Griffiths, *Introduction to Quantum Mechanics* (Prentice Hall, New Jersey, 1983).

[15] J. F. Ogilvie, *The Vibrational and Rotational Spectrometry of Diatomic Molecules* (Academic Press, San Diego, 1998) 18.

[16] S. Duckett and B. Gilbert, *Foundations of Spectroscopy* (Oxford University Press, Oxford, 2000) 23.

[17] O. Howarth, *Theory of Spectroscopy* (Halsted Press, New York, 1973) 41- 43.

[18] G. Herzberg, *Molecular Spectra and Molecular Structure: I. Spectra of Diatomic Molecules* (D. Van Nostrand Company, New Jersey, 1950).

[19] J. Vitko, Jr. and C. F. Coll, III, "Calculation of the matrix shift and center of mass frequency of H_2 and D_2 dissolved in solid argon, krypton, and xenon" *Journal of Chemical Physics* **69**, 2590-2595 (1978).

[20] W. O. George and P. S. McIntyre, *Infrared Spectroscopy* (John Wiley & Sons, Chichester, 1987) 83-85.

[21] T. Theophanides, *Fourier Transform Infrared Spectroscopy* (D. Reidel Publishing Company, Dordrecht, 1984) 148.

[22] P. R. Griffiths and J. A. de Haseth, *Fourier Transform Infrared Spectrometry* (John Wiley & Sons, New York, 1986) 199.

[23] J. L. Hunt and H. L. Welsh, "Analysis of the profile of the fundamental infrared band of hydrogen in pressure-induced absorption" *Canadian Journal of Physics* **42**, 873-885 (1964).

[24] E. U. Condon, "Production of Infrared Spectra with Electric Fields" *Physical Review* **42**, 759-762 (1932).

[25] T. C. James and W. Klemperer, "Line Intensities in the Raman Effect of $^1\Sigma$ Diatomic Molecules." *Journal of Chemical Physics* **31**, 130-134 (1959).

[26] C. Schwartz and R. J. Le Roy, "Nonadiabatic Eigenvalues and Adiabatic Matrix Elements for all Isotopes of Diatomic Hydrogen." *Journal of Molecular Spectroscopy* **121**, 420-439 (1987).

[27] D. B. Chase and J. F. Rabolt, *Fourier Transform Raman Spectroscopy: From Concept to Experiment* (Academic Press, San Diego, 1994) 228.

[28] J. D. Jackson, *Classical Electrodynamics* (John Wiley & Sons, Inc., New York, 1962). 136.